(12) INTERNATIONAL APPLICATION PUBLISHED UNDER THE PATENT COOPERATION TREATY (PCT)

(19) World Intellectual Property Organization
International Bureau

(43) International Publication Date
26 April 2007 (26.04.2007)

PCT

(10) International Publication Number
WO 2007/047624 A1

(51) International Patent Classification:
C02F 1/72 (2006.01) *C02F 1/62* (2006.01)
C02F 1/28 (2006.01)

(21) International Application Number:
PCT/US2006/040458

(22) International Filing Date: 16 October 2006 (16.10.2006)

(25) Filing Language: English

(26) Publication Language: English

(30) Priority Data:
60/726,924 14 October 2005 (14.10.2005) US

(71) Applicants *(for all designated States except US)*: **INFRAMAT CORPORATION** [US/US]; 74 Batterson Park Road, Farmington, CT 06032 (US). **UNIVERSITY OF HOUSTON** [US/US]; 4800 Calhoun Street, East Cullen Building, Room 316, Houston, TX 77204-2015 (US).

(72) Inventors; and
(75) Inventors/Applicants *(for US only)*: **CHEN, Huimin** [CN/US]; 39 Timber Lane, Willington, CT 06279 (US). **WANG, Meidong** [CN/US]; 39 Timber Lane, Willington, CT 06279 (US). **XIAO, Danny** [US/US]; 50 Hall Hill Road, Willington, CT 06279 (US). **CLIFFORD, Dennis, A.** [US/US]; 5803 Hummingbrid Street, Houston, TX 77053 (US).

(74) Agent: **SHAHRIARI, Dean**; Cantor Colburn LLP, 55 Griffin Road South, Bloomfield, CT 06002 (US).

(81) Designated States *(unless otherwise indicated, for every kind of national protection available)*: AE, AG, AL, AM, AT, AU, AZ, BA, BB, BG, BR, BW, BY, BZ, CA, CH, CN, CO, CR, CU, CZ, DE, DK, DM, DZ, EC, EE, EG, ES, FI, GB, GD, GE, GH, GM, GT, HN, HR, HU, ID, IL, IN, IS, JP, KE, KG, KM, KN, KP, KR, KZ, LA, LC, LK, LR, LS, LT, LU, LV, LY, MA, MD, MG, MK, MN, MW, MX, MY, MZ, NA, NG, NI, NO, NZ, OM, PG, PH, PL, PT, RO, RS, RU, SC, SD, SE, SG, SK, SL, SM, SV, SY, TJ, TM, TN, TR, TT, TZ, UA, UG, US, UZ, VC, VN, ZA, ZM, ZW.

(84) Designated States *(unless otherwise indicated, for every kind of regional protection available)*: ARIPO (BW, GH, GM, KE, LS, MW, MZ, NA, SD, SL, SZ, TZ, UG, ZM, ZW), Eurasian (AM, AZ, BY, KG, KZ, MD, RU, TJ, TM), European (AT, BE, BG, CH, CY, CZ, DE, DK, EE, ES, FI, FR, GB, GR, HU, IE, IS, IT, LT, LU, LV, MC, NL, PL, PT, RO, SE, SI, SK, TR), OAPI (BF, BJ, CF, CG, CI, CM, GA, GN, GQ, GW, ML, MR, NE, SN, TD, TG).

Published:
— *with international search report*
— *before the expiration of the time limit for amending the claims and to be republished in the event of receipt of amendments*

For two-letter codes and other abbreviations, refer to the "Guidance Notes on Codes and Abbreviations" appearing at the beginning of each regular issue of the PCT Gazette.

(54) Title: WATER TREATMENT COMPOSITION COMPRISING NANOSTRUCTURED MATERIALS

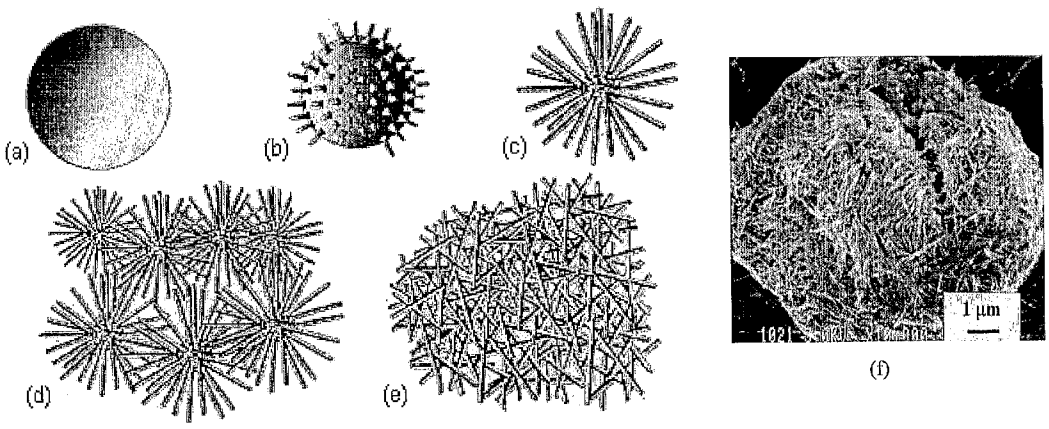

(57) Abstract: A water treatment composition containing both an oxidizing component and an absorbing component, wherein one or both comprise nanostructured materials. The nanostructured materials may be agglomerated to form particles having an average longest dimension of at least one micrometer. The oxidizing component comprises a manganese-, silver-, and/or titanium-, zirconium-, aluminium-, and/or iron-containing composition. Both constituents amy comprise an oxide, hydroxide, or oxyhydroxide and both may be doped. The water treatment compositions are useful in at least partially removing contaminants such as metallic or cationic arsenic, lead, chromium, and/or mercury from water.

WO 2007/047624 A1

WATER TREATMENT COMPOSITION COMPRISING NANOSTRUCTURED MATERIALS

CROSS REFERENCE TO RELATED APPLICATION

This application claims the benefit of United States Provisional Patent Application Serial Number 60/726,924 filed October 14, 2005, which is incorporated herein by reference in its entirety.

STATEMENT REGARDING FEDERALLY SPONSORED RESEARCH

The United States Government has certain rights to this disclosure pursuant to United States Air Force Flight Test Center Contract Nos. F04611-03-M-1007 and FA9300-04-C-0033.

BACKGROUND

[0001] The present disclosure generally relates to water treatment. More particularly, the present disclosure relates to compositions and methods for removal of contaminants from aqueous streams.

[0002] Wastewater and natural waters (e.g., surface water or groundwater) may contain a variety of dissolved inorganic substances from natural and anthropogenic sources. Regulatory limits have been set for a number of these substances in drinking water and for discharges to natural waters, for protection of public health and of environmental quality. In many locations, the regulatory limits for many of these substances are set at very low levels, e.g., about 2 to about 50 micrograms per liter (μg/L).

[0003] Current water treatment processes, such as granular iron media adsorption, modified coagulation / filtration, reverse osmosis hyperfiltration, anion exchange, activated alumina adsorption, modified lime softening, electrodialysis reversal, and oxidation / filtration, are available and cost-effective for large municipal water treatment facilities.

However, as the regulated levels of these contaminants are reduced even further, many of these processes are rendered inadequate. Furthermore, improvements on these technologies or creation of new technologies are needed for small water treatment systems (e.g., those that serve communities of 25 to 10,000 people) and point-of-use or point-of-entry systems (e.g., those for use in private wells) to treat water cost-effectively.

[0004] There accordingly remains a need in the art for improved compositions and methods for removing contaminants from aqueous streams.

BRIEF SUMMARY

[0005] Disclosed herein are water treatment compositions. In one embodiment, a water treatment composition includes an oxidizing component and an absorbing component, wherein one or both of the oxidizing component and absorbing component comprise nanostructured materials.

[0006] In another embodiment, the water treatment composition includes a nanostructured manganese containing composition and a nanostructured absorbing component, wherein the nanostructure manganese-containing composition and the nanostructured absorbing component are agglomerated to form a particle having an average longest dimension of at least one micrometer.

[0007] A method for treating water includes contacting water with the water treatment composition and at least partially removing a contaminant from the water.

[0008] The above described and other features are exemplified by the following figures and detailed description.

BRIEF DESCRIPTION OF THE DRAWINGS

[0009] Referring now to the figures, which are exemplary embodiments and wherein like elements are numbered alike:

[0010] Figure 1 schematically illustrates the transformation of MnO_2 nanoparticle agglomerates into a mass of interconnected nanofibers, starting with (a) a nanoparticle, then (b) nucleation of embryonic nanofibers, followed by (c) transformed long fibers, (d) fiber bundles, and finally (e) a fully developed bird's-nest superstructure, which is also shown in (f) a scanning electron microscope (SEM) image;

[0011] Figure 2 illustrates powder X-ray diffraction patterns for two different samples of MnO_2;

[0012] Figure 3 graphically illustrates the mesopore size distribution of MnO_2 synthesized at room temperature and 70 degrees Celsius (°C);

[0013] Figure 4 illustrates high resolution scanning electron microscope (HR-SEM) images of MnO_2 synthesized at (a) room temperature and (b) 70 °C;

[0014] Figure 5 illustrates (a) an optical microscope image of reconstituted MnO_2 particles having a particle size greater than 150 micrometers as well as (b and c) SEM images of reconstituted nanofibrous MnO_2 particles;

[0015] Figure 6 graphically illustrates the As(III) oxidation in low dissolved oxygen challenge water at a pH of about 7.5 without any interfering reductants;

[0016] Figure 7 graphically illustrates the As(III) oxidation in low dissolved oxygen challenge water at a pH of about 7.5 with Fe(II) as an interfering reductant;

[0017] Figure 8 graphically illustrates the As(III) oxidation in low dissolved oxygen challenge water at a pH of about 7.5 with Mn(II) as an interfering reductant;

[0018] Figure 9 graphically illustrates the As(III) oxidation in low dissolved oxygen challenge water at a pH of about 7.5 with sulfide as an interfering reductant;

[0019] Figure 10 graphically illustrates adsorption isortherms for As(V);

[0020] Figure 11 graphically illustrates an adsorption isortherm for Pb(II);

[0021] Figure 12 is a SEM image of a nanostructured Fe_2O_3 sample;

[0022] Figure 13; is a SEM image of a nanostructured Mn-doped Fe_2O_3 sample;

[0023] Figure 14; is a SEM image of a nanostructured La-doped Fe_2O_3 sample;

[0024] Figure 15 graphically illustrates As(V) adsorption isortherms for a composite Fe_2O_3-MnO_2 media at various pH;

[0025] Figure 16 graphically illustrates the breakthrough curves of total arsenic, As(III), and As(V) using a composite Fe_2O_3-MnO_2 media at a pH of about 7.5;

[0026] Figure 17 graphically illustrates the breakthrough curves of As(V) for a composite Fe_2O_3-MnO_2 media and GFH at a pH of about 6.5;

[0027] Figure 18 graphically illustrates the breakthrough curves of As(V) for a composite Fe_2O_3-MnO_2 media and GFH at a pH of about 7.5;

[0028] Figure 19 graphically illustrates the breakthrough curves of As(V) for a composite Fe_2O_3-MnO_2 media and GFH at a pH of about 8.5;

[0029] Figure 20 graphically illustrates the breakthrough curves of As(III) and As(V) for a composite Fe_2O_3-MnO_2 media at a pH of about 7.5;

[0030] Figure 21 graphically illustrates the breakthrough curves of As(V) for a composite Fe_2O_3-MnO_2 media, Fe_2O_3, and GFH at a pH of about 7.5;

[0031] Figure 22 graphically illustrates Pb(II) adsorption isortherms for a composite Fe_2O_3-MnO_2 media at various pH;

[0032] Figure 23 graphically illustrates the breakthrough curve of Pb(II) for a composite Fe_2O_3-MnO_2 media at a pH of about 7.5;

[0033] Figure 24 illustrates powder X-ray diffraction patterns for an as-synthesized samples of $Ti(OH)_4$ and a heat treated sample of $Ti(OH)_4$;

[0034] Figure 25 illustrates a powder X-ray diffraction pattern for an as-synthesized samples of $Zr(OH)_4$;

[0035] Figure 26 is a SEM image of a nanostructured $Zr(OH)_4$ sample;

[0036] Figure 27 is a SEM image of a nanostructured Mn-doped $Zr(OH)_4$ sample;

[0037] Figure 28 is a SEM image of a nanostructured Mn-doped $Ti(OH)_4$ sample;

[0038] Figure 29 graphically illustrates As(V) adsorption isortherms for a Mn-doped Zr-based adsorbent at various pH;

[0039] Figure 30 graphically illustrates As(V) adsorption isortherms for a Mn-doped Ti-based adsorbent at various pH;

[0040] Figure 31 graphically illustrates As(V) adsorption isortherms for a commercially available adsorbent, GFO, at various pH; and

[0041] Figure 32 graphically illustrates the breakthrough curves of As(V) for a a Mn-doped Ti-based adsorbent and GFO at a pH of about 7.5.

DETAILED DESCRIPTION

[0042] Disclosed herein are water treatment compositions and methods of making and using the water treatment compositions. The water treatment compositions are useful for removing contaminants from water. Specific contaminants include metallic or cationic arsenic, lead, chromium, mercury, or a combination comprising at least one of the foregoing.

[0043] In contrast to the prior art, the water treatment compositions generally comprise both an oxidizing component and an absorbing component. The oxidizing component and/or the absorbing component may be nanostructured. In an exemplary embodiment, both the oxidizing component and the absorbing component are nanostructured. The term "nanostructured", as used herein, refers to particles having an average longest grain dimension of less than about 250 nanometers (nm). One or both of the oxidizing component

and absorbing component comprising the nanostructured materials can be agglomerated to form particles having an average longest dimension of at least one micrometer.

[0044] The oxidizing component can include a manganese-, silver-, and/or titanium-containing composition. Suitable compositions include oxides, hydroxides, or oxyhydroxides of manganese, silver, or titanium. The absorbing component can include a titanium-, zirconium-, aluminum-, and/or iron-containing composition. Suitable compositions include oxides, hydroxides, or oxyhydroxides of titanium, zirconium, aluminum, or iron. The oxidizing component can be doped. In addition, or in the alternative, the absorbing component can be doped. It should be noted that the oxidizing component and the absorbing component must have different nominal compositions. That is, that while the oxidizing component and the absorbing component can have overlapping elements or constituents, the overall composition of each component must be different.

[0045] In an exemplary embodiment, the oxidizing component is a manganese oxide an iron-doped manganese oxide, or a combination comprising at least one of the foregoing; and the absorbing component is an iron oxide, a Mn- or La-doped iron oxide, a zirconium hydroxide, a Mn- or Fe-doped zirconium hydroxide, a titanium hydroxide, a Mn- or Fe-doped titanium hydroxide, or a combination comprising at least one of the foregoing.

[0046] Desirably, the overall water treatment composition is highly porous so as to allow the treated water to flow therethrough, yet also absorb contaminants during treatment. In an exemplary embodiment, one or both of the oxidizing component and the absorbing component has a so-called "bird's nest" fibrous structure, as shown in Figure 1 (e) and (f).

[0047] The water treatment compositions can be disposed onto a carrier and/or incorporated into a filtration device.

[0048] A method for using any of the water treatment compositions disclosed herein generally includes contacting water with the water treatment composition and at least partially removing a contaminant from the water. In one embodiment, at least partially removing the contaminant can include oxidizing the contaminant and absorbing the oxidized contaminant.

[0049] The adsorption of a contaminant onto the water treatment compositions generally occurs by ligand exchange. Advantageously, because these contaminants strongly bond to the water treatment media, the media, once exhausted, can be disposed of as a non-hazardous waste in landfills.

[0050] The disclosure is further illustrated by the following non-limiting examples.

EXAMPLE 1: Manganese Dioxide Nanofiber Synthesis and Characterization

[0051] MnO_2 was synthesized by oxidizing manganese sulfate ($MnSO_4$) with potassium permanganate ($KMnO_4$) under acidic conditions according to reaction (1).

$$2KMnO_4 + 3MnSO_4 + 2H_2O \rightarrow 5MnO_2 \downarrow + K_2SO_4 + 2H_2SO_4 \qquad (1)$$

[0052] The reaction time and temperature were adjusted to control the crystallinity, morphology and catalytic activity of the material. A schematic illustration showing the gradual transformation of MnO_2 nanoparticle agglomerates into a mass of interconnected nanofibers is shown in Figure 1. These transformations can be controlled by adjusting time and/or temperature of the reaction. It is believed that the MnO_2 is more active in the nucleation and growth stages than during the other stages.

[0053] Powder X-ray diffraction (XRD) patterns of the MnO_2 were obtained on a Bruker D5005 or D8 diffractometer equipped with a 2.2 kilowatt (kW) Cu X-ray tubes. The equipment was run at 40 kilovolt (kv) and 20 milliAmpere (mA) by step-scanning with increments of 5 degrees per minute (°/min). XRD analysis (as shown in Figure 2) revealed that synthesis temperature had a great influence on the crystallinity. The MnO_2 material synthesized at 70 degrees Celsius (°C) possessed better crystallinity than the one synthesized at room temperature (about 23°C). The peak associated with the <020> direction was narrower than all other peaks, indicating that the crystallites were elongated along the <020> direction. In addition, the broadness of this peak is associated with the length of fiber. Specifically, the broader the peak the shorter the fiber. It is apparent that the <020> peak of MnO_2 synthesized at room temperature was much broader compared with that synthesized at 70°C, suggesting that the MnO_2 synthesized at room temperature had a shorter fiber length.

[0054] Specific surface area (SSA), total pore volume, micropore volume, and mesopore size distribution of the as-synthesized MnO_2 nanofibers were analyzed on a QuantaChrome NOVA4200e surface area and pore size analyzer using the BET method. SSA and pore analyses of MnO_2 samples are listed in Table 1. Pores are classified by diameter as micropores (<10 Å), mesopores (10 to 250 Å) and macropores (>250 Å). The MnO_2 synthesized at room temperature possessed a higher SSA than the MnO_2 synthesized at 70°C, although its total pore volume was lower. This suggested that it had a smaller particle size, contained micropores, or both. The results shown in Table 1 confirmed that MnO_2 synthesized at room temperature contained micropores, which contributed about 75 square meters per gram (m^2/g) of its 259 m^2/g SSA. Mesopore size distributions of these two materials are shown in Figure 3.

Table 1. BET surface area and pore analyses

MnO_2	SSA (m^2/g)	Total Pore Volume (cc/g)	Micropore Volume (cc/g)	Micropore Area (m^2/g)	Mesopore size distribution
Room Temp	259	0.29	0.04	75	Peak at 18 Å
70°C	190	0.39	0	0	Peaks at 20 and 93 Å.

[0055] The MnO_2 synthesized at room temperature exhibited a singular pore size distribution with a pore radius peak of about 17 Angstroms (Å). In contrast, the MnO_2 synthesized at 70°C exhibited a bimodal pore size distribution with pore radii peaks at about 20 Å and about 93 Å, respectively. The 93 Å peak was much broader than the 20 Å peak; it covered a pore radius from about 50 Å to about 300 Å. Most pores in this range were interparticle voids that formed among particles. Theoretically, both micropores and mesopores are accessible for arsenic species in the water, because the radius of arsenic ions, such as AsO_4^{3-} with r = 0.47Å and H_3AsO_3 with r = 0.69 Å, are much smaller than the sizes of the observed micropores and mesopores.

[0056] High resolution scanning electron microscope (HR-SEM) images were acquired at 10 kilo-electron Volts (KeV) using a Jeol 890 inlens SEM. HR-SEM images of MnO_2 are shown in Figure 4. The MnO_2 synthesized at room temperature appeared to have a spiked ball morphology, while the MnO_2 synthesized at 70°C exhibited a nanofiber

morphology. Based on Figure 1, the MnO_2 synthesized at room temperature appeared to still be in the growing stage. This is consistent with the XRD results that the MnO_2 synthesize at room temperature had a shorter fiber length.

[0057] It was also observed that interparticle voids formed among MnO_2 spikes about 50 Å to about 300 Å. This is consistent with pore size distribution results. Optical and scanning electronic microscope images of reconstituted MnO_2 particles are shown in Figure 5. Spray drying was used to reconstitute the nanoporous MnO_2 powder. The optical microscope image in Figure 5(a) showed that the reconstituted MnO_2 particles were substantially spherical with diameters of greater than or equal to about 150 micrometers. The SEM image of the reconstituted nanofibrous MnO_2 particles in Figure 5(b) shows that each sphere comprises hundreds of agglomerated particles having a size range from submicrometers to a few micrometers. An increase in magnification, as shown in the SEM image of 5(c), shows that each agglomerate comprises a plurality of spiked balls of MnO_2, with macropores among the bundles and mesopores among the spikes.

EXAMPLE 2: Evaluation of MnO_2 for Water Treatment

[0058] In this example, the MnO_2 nanofibers synthesized according to Example 1 were evaluated for their efficiencies in oxidizing As(III) to As(V) in comparison with a commercially available product. The comparisons were made using rapid small scale column tests (RSSCTs) under a variety of experimental conditions. Using adsorption isotherm tests, MnO_2 nanofibers were also evaluated for their performance in removing As(V) and Pb(II) from drinking water.

[0059] For all evaluation experiments, a so-called "challenge water" of the composition described in Table 2 was used. It has the same anionic composition as the National Sanitation Foundation (NSF) International Standard 53 Challenge Water used for evaluation of point-of-use devices for arsenic removal. Its calcium and magnesium concentrations were lowered to give the water greater long-term stability, as the NSF water is stable only for about 24 to about 48 hours, whereas the isotherm tests described herein were conducted for greater than or equal to about 48 hours. The following reagent grade salts were used to prepare the challenge water: $NaNO_3$, $NaHCO_3$, Na_2HPO_4 H_2O, NaF, $Na_2SiO_3 \cdot 9H_2O$,

$MgSO_4 \cdot 7H_2O$, and $CaCl_2 \cdot 2H_2O$. Interfering Fe^{2+} ions in As(III) oxidation tests were introduced from ferrous ammonium sulfate (EM Science). Mn^{2+} and S^{2-} were prepared from $MnSO_4$ H_2O, and Na_2S $9H_2O$, respectively.

Table 1. Composition of the Challenge Water

Cations	meq/L	mg/L	Anions	meq/L	mg/L
Na^+	3.604	82.9	HCO_3^-	2.0	122.0
Ca^{2+}	0.36	7.21	SO_4^{2-}	1.0	48.0
Mg^{2+}	0.26	3.16	Cl^-	0.36	12.8
			NO_3^--N	0.143	2.0
			F^-	0.053	1.0
			PO_4^{3-}-P	0.0013	0.04
			Silicate as SiO_2	0.66	20.0
Total	4.224	93.27		4.224	205.8

Estimated total dissolved solids (TDS) by evaporation = 287 mg/L.
meq/L = milliequivalents per liter
mg/L = milligrams per liter

[0060] Both low and high levels of dissolved oxygen (DO) were used in the challenge water during As(III) oxidation tests. Low-DO, i.e., less than about 80 parts per billion (ppb) O_2, challenge water was prepared by sparging the challenge water with N_2 for 1.5 hours. High-DO challenge water was prepared by sparging water with air for 15 minutes to a dissolved oxygen saturation concentration of approximately 8.3 mg/L. As(III) was spiked into the challenge water, and then freshly prepared Fe^{2+}, Mn^{2+} or S^{2-} solutions were spiked. During the experiments, the pH of the challenge water was adjusted to a range of about 6.5 to 8.5 by using dilute HCl and NaOH solutions.

[0061] For the As(III) oxidation tests, rapid small scale column tests (RSSCTs) were used to evaluate MnO_2 nanofibers for their efficiency in oxidizing As(III) to As(V). The tests were conducted under a variety of experimental conditions including variable pH, empty bed contact time (EBCT), low/high dissolved oxygen (DO), and the absence or presence of interfering reductants (Fe^{2+}, Mn^{2+}, or S^{2-}).

[0062] It is noted here that MnO_2 nanofibers were not directly used in the column test, because of their small particle size (about 10 μm) which would have given an extremely high pressure drop in a packed bed. To achieve reasonable RSSCT flow rates, the MnO_2 nanofibers were granulized by the spray-drying technique described in Example 1 to form

larger, but porous particles. Granulized, porous MnO_2 particles (having diameters of about 125 to about 180 μm) were loaded into a 1 centimeter inner diameter glass column with total volume of 1.0 mL. The column was then backwashed with deionized water to remove fines.

[0063] The As(III) oxidation tests were conducted by pumping the Low-DO challenge water containing As(III) through the column at a controlled flow rate. To speciate the effluent, 10-mL samples of the effluent from the RSSCT were collected and preserved with EDTA-HAc. As(III) concentration in the effluent was analyzed by hydride-generation atomic absorption spectrophotometry (HG-AAS).

[0064] For the As(V) and Pb(II) adsorption isotherm testes, a 2-day wet-slurry isotherm procedure was used for adsorption isotherm tests. First, adsorbents were screened with a set of 200 and 325 mesh sieves. Powder that was trapped between these two sieves, i.e., having a particle size between about 45 to about 75 μm, was used to make a suspension with a powder content of 1.00 g/L. The suspension was vigorously stirred to keep powders suspended. Predetermined aliquots of the vigorously stirred suspension were pipetted into 150-mL bottles to yield appropriate adsorbent concentrations for the equilibrium adsorption tests. Then, 100-mL aliquots of As(V) or Pb(II) spiked synthetic water was added to each bottle. Adsorbent media dosages that were tested were: 0, 0.25, 0.5, 1, 2, and 5 mg MnO_2 in every 100 mL As(V) or Pb(II) spiked synthetic water. The dosed bottles and the blank (no adsorbent) were placed in a covered wooden box and rotated at 15 revolutions per minute (rpm) for 2 days at ambient temperature (about 23°C) to reach adsorption equilibration. It was determined that a reasonable approach to equilibrium was reached in 48 hours. After the equilibration, a 10-mL water sample was collected from each bottle and microfiltered with a 0.2 μm filter disc to remove all suspended particles (adsorbent media). The water samples were preserved with concentrated HNO_3 prior to analysis. The acid concentration in the water sample was about 1% (v/v). For As(V) adsorption isotherm tests, the challenge water was spiked with 200 μg/L As(V). Arsenic concentrations in the preserved water samples were also measured by HGAAS. The mass of arsenic adsorbed onto the media was determined from the difference in soluble arsenic concentrations in the equilibrated samples and the blank (no adsorbent). For Pb(II) adsorption isotherm tests, the challenge water was spiked with 500 μg/L Pb(II), and the Pb(II) concentrations in the preserved water samples

were measured by inductively coupled plasma mass spectrometry (ICP-MS). The mass of lead adsorbed onto the media was determined from the difference in soluble lead concentrations in the equilibrated samples and the blank (no adsorbent).

[0065] The arsenic analysis was performed using a Perkin-Elmer (Model Zeeman 5000) atomic absorption spectrometer (AAS) coupled with a Perkin-Elmer FIAS-100 unit for hydride generation for the determinations of As(III) and As(total). The arsenic lamp was an electrodeless discharge lamp (EDL) operated at 8W from an external power supply. To determine total arsenic, water samples were treated with L-cysteine in a 2 moles per liter (M) HCl solution to reduce As(V) to As(III) which was determined by the HGAAS. For the determination of As(III) in the presence of As(V), the carrier HCl solution was replaced by a 2 M citric/citrate buffer solution at a pH of about 5.0. Arsine was generated using 0.2% sodium tetrahydroborate in 0.05 % NaOH. Under these condition As(V) was not converted to AsH_3 and did not interfere in the determination of As(III). As(V) was calculated from the difference between As(total) and As(III). The detection limit (DL) was 0.04 μg/L for As(total) and 0.096 μg/L for As(III).

[0066] Short-term As(III) oxidation tests at high-DO were conducted to compare the efficiency of a commercially available MnO_2, FILOX-R, with nanoporous MnO_2 in oxidizing As(III) to As(V) at three different EBCTs (2.0, 1.0, and 0.50 minutes) and at two pHs (8.3 and 6.5). Both FILOX-R and naofibrous MnO_2 granules completely oxidize As(III) to As(V). No distinguishable performance was observed under these test conditions.

[0067] In the short-term, low-DO experiments, the EBCT was further reduced to about 0.125 minutes to differentiate the oxidizing efficiencies of both media. Table 3 compares the performances of FILOX-R and granulated nanofibrous MnO2 media at different EBCTs for low-DO challenge water without any interfering reductant at pH 8.3 and 7.5. Up to about 0.25 minutes EBCT there was no significant difference in oxidizing performance between the two media. But there was a clear difference in the As(III) oxidation rate at an EBCT of 0.125 minutes. Granulated nanofibrous MnO2 media was more effective than FILOX-R for rapid oxidation of As(III) to As(V). At higher pH both media showed

better performance than at lower pH; at both pHs the oxidizing efficiency of granulated nonofibrous MnO2 media was better than FILOX-R.

[0068] Based on the short-term experiments at low and high-DO, it could be concluded that DO had no significant effect on oxidizing efficiency up to EBCT 0.5 minutes for both media.

Table 3. As(III) oxidation performance of FILOX-R and Inframat media at low-DO without any interfering reductants

Challenge Water pH	EBCT	Percent oxidation of As(III)	
		FILOX-R	MnO_2 Granules
pH 8.3	0.5	100	100
	0.25	98	100
	0.125	79	94
pH 7.5	0.125	71	75

[0069] Long term experiments with interfering reductants were carried out. To study the effects of the interfering reductants, except sulfide, on the oxidation performance, a run length of more than 2100 bed volumes (BV) was considered. In the presence of sulfide, arsenic sulfides along with many water-soluble thioarsenite species are formed, and accurate differentiation between As(III) and As(V) cannot be made. The availability of the free As(III) decreased with time. So, in the presence of sulfide, only short-term experiments were conducted to observe the effects of sulfide on oxidizing efficiency of the granulated nanoporous material and FILOX-R.

[0070] In the absence of interfering reductants, the results of the longer-term oxidation performances of nanofibrous MnO_2 granules and FILOX-R are shown in Figure 6. The tests were performed at an EBCT of about 0.125 minutes, low-DO, and at pH 7.5. As(III) oxidation was greater than or equal to about 70% throughout the 3280 BV run length with when nanofibrous MnO_2 granules were used. As a reference, about 3500 BV is approximately equivalent to about 438 minutes run time.

[0071] As can be seen in Figure 6, the FILOX-R had a slightly lower oxidizing efficiency than the nanofibrous MnO_2 granules under the same experimental conditions. Therefore, in the absence of any interfering reductant, both media can effectively oxidize As(III) under low-DO condition, however, the nanofibrous MnO_2 granules showed slightly better oxidative performance FILOX-R.

[0072] When 2.0 mg/L Fe(II), as an interfering reductant, was present in the feed, As(III) oxidation was reduced for a short period of time for nanofibrous MnO_2 granules, and then the efficiency decreased slowly to about 1200 BV. After about 1200 BV, the oxidative ability was substantially constant. With FILOX-R, initially up to about 240 BV, Fe(II) had no effect on As(III) oxidation, but after about 240 BV, the oxidative efficiency decreased gradually up to about 2160 BV. These results, which are shown in Figure 7 for a pH of about 7.5 and an EBCT of 0.125 minutes, clearly indicated that nanofibrous MnO_2 outperformed FILOX-R in the presence of Fe(II).

[0073] The effect of 0.2 mg/L Mn(II) as an interfering reductant on both media's As(III) oxidation efficiency was studied at a pH of about 7.5 and an EBCT of 0.125 minutes, and the results are shown in Figure 8. As indicated by Figure 8, , initially up to about 120 BV, the oxidation efficiencies of the nanofibrous MnO_2 granules and FILOX-R increased slightly and then decreased slightly with increasing BV treated. The experimental results indicate a slight advantage for nanofibrous MnO_2 compared with FILOX-R.

[0074] When both As(III) and sulfide are present in anoxic water insoluble sulfides and soluble sulfide complexes are formed. It has previously been determined that under anoxic conditions in the presence of sulfide, As(III) forms insoluble As_2S_3 and soluble thioarsenite species depending on the pH of the solution and the concentrations of As(III) and S^2. Therefore, in waters containing sulfide and As(III), colloidal and anionic forms of As(III) are expected, which render the current As(III)/(V) speciation methods inapplicable. Oxidation of As(III) to As(V) cannot be accurately determined in these waters using the EDTA-HAc preservation speciation method that was used for the As(III) oxidation studies in the absence of sulfide. Thus, the differential-pH hydride generation speciation method was

employed to overcome the analytical problem with As(III/V) preservation-speciation in the presence of sulfide.

[0075] The oxidation efficiencies of the nanoporous MnO_2 and FILOX-R were calculated at specified time intervals and compared in Figure 9 for 2.0 mg/L sulfide, a pH of about 7.5, and an EBCT of about 0.125 minutes. The results indicated that in both cases the oxidation efficiencies decreased with increasing BV. The results also indicated that in the presence of sulfide, FILOX-R slightly outperformed the nanofibrous MnO_2 granules.

[0076] The ability of MnO_2 to adsorb As(V) from the challenge water was evaluated using batch isotherms tests. As(V) adsorption isotherms of MnO_2 are shown in Figure 10 for both the nanoporous MnO_2 and a commercially available iron-based arsenic adsorbent, GFH. As can be seen from the data of Figure 10, more arsenic was removed when a higher dosage of the adsorbent was added, resulting in a lower residual (equilibrium) arsenic concentration. Adsorption capacity was calculated by dividing arsenic concentration difference before and after adsorption equilibrium by the amount of adsorbent added. After developing the isotherms, the data were fitted to the Freundlich equation (2):

$$q_e = KC_e^{1/n}, \text{ where} \qquad (2)$$

K = Freundlich constant indicative of adsorption capacity of adsorbent (L/μg)

C_e = Equilibrium concentration (μg/L)

q_e = Mass of arsenic adsorbed per mass of the adsorbent (mg/g)

n = Experimental constant indicative of adsorption intensity of the adsorbent

[0077] The As(V) adsorption capacity of MnO_2 is substantial, although not as high as GFH. MnO_2 is a good oxidant for As(III) to As(V), but was not expected to have good As(V) adsorption capacity. The unusually high As(V) adsorption capacity that was found for the MnO_2 nanofibers is believed to be related to its high surface area.

[0078] Finally, the ability of MnO_2 to adsorb Pb(II) from the challenge water was evaluated using batch isotherms tests. The Pb(II) adsorption isotherm for nanofibrous MnO_2 is shown in Figure 11. This material possesses a much higher adsorption capacity for Pb(II)

(90 μg/g at 50 μg/L Pb(II)) compared with to As(V) (4.5μg/g at 50 mg/L As(V)). The fact that MnO_2-based media adsorbs more Pb(II) than As(V) is expected because of the low point of zero charge (PZC) of MnO_2. The PZC of MnO_2 is near pH 3.0. When MnO_2 is soaked in an aqueous solution, it developed a negatively charged surface which is benefited by adsorbing positively charge species in water, such as Pb(II).

[0079] From the experiments in this example, it was concluded that the nanofibrous MnO_2 not only possessed a high efficiency in converting As(III) to As(V), but also a relatively high adsorption capacity for As(V) and Pb(II).

EXAMPLE 3: Iron Oxide Synthesis and Characterization

[0080] Fe_2O_3 was synthesized by preheating 100 mL water in a beaker to about 90 °C. A 6M NaOH solution and 100 mL of a 2M $Fe(NO_3)_3$ solution were co-precipitated into the hot water while it was continuously heated and stirred. The pH of the precipitate was controlled at about 7.5. The precipitate was continuously refluxed at about 90 °C for 6 hours. The precipitate was then filtered, washed with water, and dried in an oven at about 100 °C. The dried material was ground into a powder for further testing.

[0081] The SSA and pore analysis of this material was conducted using BET method as described in Example 1. The SSA of this material was about 154 m^2/g and the total pore volume was about 0.21 cm^3/g. XRD analysis revealed that this material possessed the α-Fe_2O_3 structure. The PZC of this material was at a pH of about 8.4. Figure 12 is an SEM image, which shows agglomerates of about 100 to about 1000 nm, comprising Fe_2O_3 particles having an average size of about 20 nm.

EXAMPLE 4: Doped Iron Oxide and Doped Manganese Oxide Synthesis and Characterization

[0082] A Mn-doped Fe_2O_3 was made following the process of Example 3 except that 8.73 g $MnSO_4 \cdot H_2O$ was dissolved into 30 mL water and was mixed with 100 mL of the 2M $Fe(NO_3)_3$ solution before the precipitation was conducted. Doping dramatically changed the material's properties. The SSA of this material was about 259 m^2/g and the total pore volume was about 0.48 cm^3/g. XRD analysis revealed that this material had the structure of a

ferrihydrate. The PZC of this material was at a pH of about 7.1. Figure 13 is an SEM image, which shows smaller agglomerates, comprising the Mn-doped Fe_2O_3 particles having an average size of about 20 nm. The smaller agglomerate size is in agreement with the higher total pore volume.

[0083] A La-doped Fe_2O_3 was made following the process of Example 3 except that $LaCl_3$ was dissolved in water and was mixed with 100 mL of the 2M $Fe(NO_3)_3$ solution before the precipitation was conducted. The SSA of this material was about 174 m^2/g and the total pore volume was about 0.41 cm^3/g. XRD analysis revealed that this material had the structure of hematite. The PZC of this material was at a pH of about 8.8. Figure 13 is an SEM image, which shows smaller agglomerates, comprising Fe_2O_3 particles having an average size of about 20 nm. Figure 14 is an SEM image of the La-doped Fe_2O_3. Similar to the Mn-doped Fe_2O_3 sample, the agglomerates are significantly smaller than those of the undoped Fe_2O_3 sample. The average particle size is about 20 nm.

[0084] A Fe-doped MnO_2 was made following the process of Example 1, with the exception that $Fe(NO_3)_3$ was used as a precursor and was added simultaneously into a beaker containing hot water with the $MnSO_4$ and the $KMnO_4$. The SSA of this material was about 503 m^2/g and the total pore volume was about 0.44 cm^3/g. XRD analysis revealed that doping reduced the crystallinity of the MnO_2 structure. The PZC of this material was at a pH greater than 3.0, which is the PZC pH for the undoped MnO_2 of Example 1.

EXAMPLE 5: Iron- and Manganese-based Nanocomposite Water Treatment Media

[0085] Various composites were prepared using the iron oxides and manganese oxides (both undoped and doped) described herein. The general procedure included dispersing about 1600 g of an iron oxide composition (doped or undoped) 1L water. Next, about 400 g of a nanofibrous manganese oxide composition (doped or undoped) were added into the iron oxide suspension and mixed using high power mechanical stirrer. About 2 weight percent (wt %) of a binder was added and mixed. The slurry was spray dried to form nanocomposite granules with a controlled particle size.

[0086] RSSCTs were carried out on a variety of samples. The first experiment studied the oxidation and adsorption efficiency of As(III) using composite Fe_2O_3-MnO_2 (Sample No. 072105-B) media at pH 7.5. The second experiment determined the breakthrough of As(V) using Fe_2O_3-MnO_2 (072105-B) media at pHs 6.5, 7.5, and 8.5, and compared them with the As(V) breakthrough of the commercially available benchmark, GFH. The third experiment determined the breakthrough of As(V) using Mn-doped Fe_2O_3 (072105-A) media at pH 7.5.

[0087] For these RSSCTs, a 1 cm inner diameter glass column containing 4 cm^3 of the media (60X40 mesh), which was carefully loaded into the column, was used. Similar glass columns were prepared for GFH. A peristaltic pump was used to pump the feed solution through the columns at a flow rate of about 8 mL/min (EBCT of about 0.5 min). Arsenic-containing challenge water was analyzed for total arsenic or As(III) in the effluent and feed solutions. All samples were preserved with concentrated HNO_3 (1 mL/L) or EDTA-acetic acid (1.34 mM EDTA and 87 mM acetic acid) when speciated. RSSCTs were conducted at different pHs using As(V) and As(III). Table 4 presents the experimental conditions for the RSSCTs.

Table 4. Experimental conditions for RSSCTs for arsenic.

Expt. no	pH	As in feed soln	EBCT (min)	Media
1	7.5	As(III)	0.5	Fe_2O_3-MnO_2 (072105-B)
2	6.5	As(V)	0.5	Fe_2O_3-MnO_2 (072105-B) and GFH
3	7.5	As(V)	0.5	Fe_2O_3-MnO_2 (072105-B) and GFH
4	8.5	As(V)	0.5	Fe_2O_3-MnO_2 (072105-B) and GFH
5	6.5	As(V)	0.5	GFH
6	7.5	As(V)	0.5	GFH
7	8.5	As(V)	0.5	GFH
8	7.5	As(V)	0.5	Fe_2O_3 (072105-A)

[0088] RSSCTs were conducted to study the oxidation of As(III) and adsorption of arsenic using the composite Fe_2O_3-MnO_2 (072105-B) media at a pH of about 7.5 at an EBCT of about 0.5 minutes. The arsenic breakthrough curves of the RSSCTs are shown in Figure 16, which indicates that at pH 7.5, the composite material significantly oxidized As(III).

As(III) concentrations in the effluent were measured after preservation with EDTA-HAc followed by differential pH HG-AAS. At about 25,000 BV the concentration of As(III) in the effluent was about 5 μg/L. As(Tot) and As(V), that is, the difference between As(Tot) and As(III), were also measured in the effluent. The As(Tot) and As(V) breakthroughs at 10 μg/L using the composite Fe_2O_3-MnO_2 media at a pH of about 7.5 were about 14500 and about 15300 BV, respectively. From this study, it was concluded that the composite Fe_2O_3-MnO_2 media was very efficient for As(III) oxidation and As(V) adsorption. In Example 2, it was shown that the MnO_2 media efficiently oxidized As(III). This composite material contained the MnO_2 of Example 2, which efficiently oxidized As(III), and Fe_2O_3, which efficiently adsorbed As(V).

[0089] Next, RSSCTs were conducted using composite Fe_2O_3-MnO_2 (072105-B) media and GFH at three different pHs at an EBCT of 0.5 min (Experiments 2-7 in Table 4). Fifty parts per billion (μg/L) As(V) was used in all experiments to evaluate the effectiveness of the composite media and the GFH. The As(V) adsorption isotherms for the composite Fe_2O_3-MnO_2 (072105-B) media at pHs of about 6.5, about 7.5, and about 8.5 are shown in Figure 15. The arsenic breakthrough curves of the column runs are shown in Figures 17, 18, and 19, for pHs of about 6.5, about 7.5, and about 8.5, respectively. The data indicated that the arsenic breakthrough curves were pH dependent, and at all three pHs, the composite Fe_2O_3-MnO_2 material significantly outperformed the GFH at 10 μg/L As(V) breakthrough. At a pH of about 6.5, both media performed better than at the higher pHs. The As(V) breakthroughs at pHs of about 6.5, about 7.5, and about 8.5 for the composite Fe_2O_3-MnO_2 media were about 25300, about 16200, and about 9900 BV, respectively. In contrast, for GFH, the As(V) breakthrough values at 10 μg/L were about 15800, about 10800, and about 6400 BV, respectively. From this data, it was concluded that the composite Fe_2O_3-MnO_2 (072105-B) media performed significantly better than the commercially available GFH media.

[0090] It has been documented that As(V) is more efficiently removed than As(III). Thus, it is important to compare the arsenic removal efficiency of the composite Fe_2O_3-MnO_2 (072105-B) media for a pure As(V) feed compared with a pure As(III) feed. Figure 20 illustrates the breakthrough curves at a pH of about 7.5 with an EBCT of about 0.5 minutes

for both As(III) and As(V). Figure 11 indicates that the composite material was almost equally efficient in removing As(III) and As(V). This means that when pure As(III) was fed into the column, the composite Fe_2O_3-MnO_2 media was doing an excellent job of oxidizing As(III) to As(V) prior to adsorption of the As(V). An advantageous feature of the composite media was that there was no need for a pre-oxidation step when arsenic was present as As(III) in the water. Advantageously, this will result in a reduction in the amount of byproducts that are generated during the pretreatment process.

[0091] The Fe-based media produced in Examples 3 and 4 were also used to study the removal efficiency of arsenic. RSSCTs were conducted using an Fe-based media (072105-A) at a pH of about 7.5 at an EBCT of about 0.5 minutes and compared with the composite Fe_2O_3-MnO_2 media (070521-B) and GFH. The results are shown in Figure 21, which indicate that Fe-based media (072105-A) alone performed significantly better than the GFH. Furthermore, the Fe-based media alone also performed similar to the composite Fe_2O_3-MnO_2 media (070521-B).

[0092] Finally, Pb(II) absorption isotherms and breakthrough curves were obtained for the composite Fe_2O_3-MnO_2 media. 500 μg/L Pb^{2+} spiked NSF 53 challenge water was used. The 2-day isotherms at pHs of about 6.5, about 7.5, and about 8.5 are shown in Figure 22. The data indicates that the media possess high Pb(II) adsorption capacities. The maximum adsorption capacity was obtained at a pH of about 8.5 and the minimum was at a pH of about 6.5. pH-dependant adsorption of Pb(II) was expected because Pb(II) is a cationic species in water and it can exchange for protons on the surface of the media. The breakthrough of Pb(II) using the composite Fe_2O_3-MnO_2 (072105-B) media at a pH of about 7.5 was conducted with 200 ppb Pb(II) spiked NSF 53 challenge water. The results are shown in Figure 23. No sign of breakthrough was shown even after about 60,000 BV run length, indicating that this media was highly effective in removing Pb(II) from water.

EXAMPLE 6: Zirconium Hydroxide and Titanium Hydroxide Synthesis and Characterization

[0093] Zirconium hydroxide, titanium hydroxide, and their doped forms were synthesized via co-precipitation of appropriate salt precursors with caustic solution similar to what was described above in Examples 1, 3 and 4. The salts used for the synthesis of

zirconium hydroxide and titanium hydroxide were $ZrOCl_2$ and $TiOSO_4$, respectively. Dopants were introduced from corresponding salt precursors that were homogeneously mixed with $ZrOCl_2$ or $TiOSO_4$ solutions. To achieve steady and controllable reaction conditions, the precursors were added simultaneously into vigorously stirred water. The flow rates of both solutions were adjusted so that the pH of the produced hydroxide slurry was at a target value throughout the reaction. The hydroxides were then filtered and washed thoroughly with deionized water to remove unwanted byproducts, and finally dried overnight in an oven at 120 °C.

[0094] The SSA and total pore volume data for zirconium hydroxide, titanium hydroxide, and their doped forms are listed in Table 5. Doped hydroxides a significantly increase higher surface area than their undoped counterparts. Titanium-based media exhibited a significantly greater SSA than the zirconium-based media. The total pore volume of titanium-based materials is also higher than that of zirconium-based materials, which suggested that titanium-based media were more porous than zirconium-based media.

Table 5. BET, SSA, and Pore Analysis Results

Sample ID.	Material Description	SSA (m^2/g)	Pore Volume (cm^3/g)	Micropore Volume (cm^3/g)	Surface Area From Micropores (m^2/g)
I-1052-050304	Zirconium hydroxide	71	0.06	0.02	47
I-1052-92804	Mn-doped zirconium hydroxide	197	0.20	0.06	92
120904	Fe-doped zirconium hydroxide	197	0.16	0.06	130
I-1052-80504	Titanium hydroxide	306	0.19	0.12	238
I-1052-092404A	Mn-doped titanium hydroxide	447	0.47	0.1	178
120204A	Fe-doped titanium hydroxide	370	0.36	0.04	76

[0095] The data revealed that undoped $Ti(OH)_4$ possesses a considerable amount of micropores (greater than about 60%), which contribute approximately 78% of its total surface area. Doping with manganese significantly increased total pore volume of $Ti(OH)_4$, while the micropore volume decreased slightly from about 0.12 cm^3/g to about 0.10 cm^3/g. This suggested that the doping created a significant amount of mesopores, resulting in a higher SSA. Compared to $Ti(OH)_4$, $Zr(OH)_4$ is less porous; but, like $Ti(OH)_4$, the porosity is significantly increased when doped. To summarize, doping has shown to be effective in increasing pore volume of these materials.

[0096] The PZCs of zirconium hydroxide and titanium hydroxide powders were found to be at pHs of about 8.08 and about 8.15, respectively. Doping with Mn slightly increased the PZCs of these materials to pHs of about 8.50 and about 8.24, respectively. When these materials were in contact with aqueous solutions that had pHs lower than their PZC, the surfaces of these materials developed a positive charge and encouraged the adsorption of negatively charged species in water, such as $H_2AsO_4^-$, $HAsO_4^{2-}$, and AsO_4^{3-}. The pH of drinking water is around 7.5. Thus, these two materials are expected to be able to quickly adsorb $H_2AsO_4^-$, and $HAsO_4^{2-}$ from drinking water.

[0097] XRD analysis on these samples revealed that the as-synthesized titanium hydroxide is amorphous, but transforms into the anatase structure type of TiO_2 after a 600 °C heat treatment for about 2 hours. The powder XRD patterns are shown in Figure 24. Similarly, the as-synthesized zirconium hydroxide is amorphous, as shown in the XRD pattern in Figure 25.

[0098] SEM images of undoped zirconium hydroxide, Mn-doped zirconium hydroxide, and Mn-doped titanium hydroxide are shown in Figures 26, 27, and 28, respectively. For easy comparison, the images are shown at the same magnification. Figure 26 indicates that the zirconium hydroxide particles have an average size of about 20 nm, which agglomerate, forming mesopores and macropores between particles. The agglomeration in the Mn-doped zirconium hydroxide, shown in Figure 27, appears to be to a lesser extent compared with the undoped sample, resulting in a higher total pore volume. No

changes in particle size were observed for this sample. Finally, the Mn-doped titanium hydroxide had an average particle size of about 10 nm. These agglomerates, as shown in Figure 28, do not appear to be as porous as was indicated by pore analysis results. This is due to the material having a significant amount of micropores that are smaller than about 2 nm, which are not visible in the SEM image.

EXAMPLE 7: Evaluation of Titanium- and Zirconium-based Absorbing Components

[0099] In this example, adsorption isotherm tests were used as screening tests to identify the titanium-based and zirconium-based media that possessed the highest As(V) adsorption capacity from each group. The selected media were further evaluated for As(V) adsorption performance under various pHs and influence of competing ions. Finally, rapid small scale column tests were conducted to compare As(V) breakthrough of the selected media and compared with a commercially available benchmark iron-based adsorbent, Granular Ferric Oxide, or GFO.

[00100] The particle size of the as-synthesized powders was about 10 micrometers in diameter, which was not directly applicable for column tests. The nanoscale powders were reconstituted into porous spherical particles with an average particle size of approximately 200 micrometers in diameter.

[00101] Six different materials, including nanoporous $Zr(OH)_4(s)$ and $Ti(OH)_4(s)$ and their doped forms, were screened using two-day isotherm tests in 200 µg/L As(V) spiked NSF Challenge Water at pH 7.5, as described above in Examples 2 and 5. Dosages of materials in the 2-day isotherms tests and the results are listed in Table 6 and 7 for the zirconium samples and the titanium samples, respectively.

Table 6. Dosage of Zr-based materials in 2-day isotherms tests and the results

dosage (mg/L)	Sample ID	Ce	qe	Sample ID	Ce	qe	Sample ID	Ce	qe
0	Z-A-0	189.58	0.00	Z-B-0	192.04	0.00	Z-C-0	200.47	0.00
10	Z-A-1	143.10	4.65	Z-B-1	183.94	0.81	Z-C-1	179.33	2.11
20	Z-A-2	83.24	5.32	Z-B-2	170.92	1.06	Z-C-2	153.89	2.33
40	Z-A-4	48.13	3.54	Z-B-4	138.79	1.33	Z-C-4	110.61	2.25
80	Z-A-8	9.40	2.25	Z-B-8	110.29	1.02	Z-C-8	51.51	1.86
100	Z-A-10	6.76	1.83	Z-B-10	88.24	1.04	Z-C-10	36.05	1.64

Sample ID: Z = Zirconium compound; A = Mn-doped, B = undoped, and C = Fe-doped; and the number indicates dosage.

Table 7. Dosages of Ti-based materials in 2-day isotherms tests and the results

dosage (mg/L)	Sample ID	Ce	qe	Sample ID	Ce	qe	Sample ID	Ce	qe
0	T-A-0	194.94	0	T-B-0	196.55	0.00	T-C-0	200.58	0.00
10	T-A-1	180.88	1.40	T-B-1	190.12	0.64	T-C-1	191.93	0.86
20	T-A-2	163.21	1.59	T-B-2	179.28	0.86	T-C-2	175.35	1.26
40	T-A-4	112.13	2.07	T-B-4	143.53	1.33	T-C-4	145.80	1.37
80	T-A-8	60.66	1.68	T-B-8	113.48	1.04	T-C-8	93.98	1.33
100	T-A-10	40.44	1.54	T-B-10	87.98	1.09	T-C-10	83.71	1.17

Sample ID: T = Titanium compound; A = Mn-doped, B = undoped, and C = Fe-doped; and the number indicates dosage.

[00102] From the As(V) adsorption isotherms of zirconium-based media, it was clear that the Mn-doped zirconium sample possessed the highest adsorption capacity, followed by the Fe-doped media. Undoped media had the lowest adsorption capacities. Like their zirconium counterparts, the Mn-doped titanium-based media outperformed Fe-doped and undoped titanium-based media. Thus, Mn-doped Zr-based and Mn-doped Ti-based media were selected for further evaluation under pH variations and the influence of competing ions.

[00103] The ability of these media to adsorb arsenic (V) from the challenge water was evaluated using batch isotherms tests. After developing the isotherms, the data were fitted to the Freundlich equation (2), shown above. The As(V) adsorption isotherm experiments were carried out using common background ions in the solution at three different pHs.

[00104] Figure 29 gives the 2-day As(V) adsorption isotherms of the Zr-based material. Figure 30 shows the As(V) adsorption capacity of Ti-based material at pHs of about 6.5, about 7.5 and about 8.5. For comparison, the 2-day As(V) adsorption isotherms of GFO at the three different pH's are shown in Figure 31. As indicated by the data, the As(V) adsorption capacities of the three materials were highest at a pH of about 6.5, with progressively less adsorption of arsenic at a pH of about 7.5 and about 8.5. Irrespective of pH, the GFO exhibited the highest As(V) adsorption capacity among the adsorbents. The Zr-based material exhibited a higher capacity than the Ti-based material at all pHs.

[00105] Batch isotherm tests with the NSF challenge water were conducted on the Mn-doped Zr- and Ti-based media at different pH's, with varying concentrations of competing ions including silica (5 and 20 mg/L) and phosphate (0 and 40 μg/L).

[00106] First, two-day adsorption isotherms were performed with the challenge water containing 40 μg/L of phosphate (P). These results were compared with challenge water without phosphate (P = 0 μg/L). For the GFO, phosphate did not have a significant impact on the As(V) adsorption capacity of GFO. Though slightly better adsorption capacities were obtained in the absence of phosphate, it was not significant enough to say that, in the presence of silicate and other background ions, phosphate ions compete with the As(V) for adsorption sites at the tested concentration. The Mn-doped Zr- and Ti-based media followed similar trends. That is, there was no significant difference in absorption between the presence and absence of phosphate in the challenge water containing silicate and other background ions. The summary of the experimental results are presented in Table 8, from which it was concluded that the presence of phosphate did not reduce the adsorption capacities of the adsorbents.

Table 8. Comparison of As(V) removal capacities of media at C_e = 50 μg/L

	pH 6.5		pH 7.5		pH 8.5	
Media	P = 0 μg/L	P = 40 μg/L	P = 0 μg/L	P = 40 μg/L	P = 0 μg/L	P = 40 μg/L
GFO	9.32	8.35	8.7	7.22	6.35	5.59
Zr-based	6.86	7.1	3.95	4.12	3.08	2.3
Ti-based	2.37	2.19	1.9	1.67	1.61	1.43

[00107] Next, experiments were performed using the challenge water with the standard concentration of silica (about 20.0 mg/L) and with low silica (about 5.0 mg/L) concentrations to study the effect of silica on adsorption capacities of the GFO, Zr-based and Ti-based media at pHs from about 6.5 to about 8.5. The data is summarized in Table 9. Each of the materials performed better (i.e., adsorbed more As(V)) at the lower concentration of silica. At the higher concentration of silica, the silica competed with As(V) ions for sites on the adsorbents. At a pH of about 6.5 and a silica concentration of about 5.0 mg/L, the Zr-based media exhibited a slightly higher As(V) adsorption capacity than the GFO. The

presence of silica greatly reduced the adsorption capacity of the Zr-based material. Under all other conditions, the As(V) adsorption capacity of the Zr-based media was much greater than that of Ti-based media.

Table 9. Comparison of As(V) removal capacities (in μg As(V)/mg) at C_e = 50 μg/L with silica at 5 and 20.0 mg/L

	pH 6.5		pH 7.5		pH 8.5	
Media	Si = 5.0 mg/L	Si = 20.0 mg/L	Si = 5.0 mg/L	Si = 20.0 mg/L	Si = 5.0 mg/L	Si = 20.0 mg/L
GFO	9.79	8.35	8.1	7.22	7.2	5.59
Zr-based	10.1	7.1	7.09	4.12	5.2	2.3
Ti-based	3.46	2.19	2.57	1.67	2.29	1.43

[00108] RSSCTs were carried out to determine the relative breakthroughs of As(V) for the Zr-based media and the benchmark media, GFO at a pH of about 7.5. The RSSCTs were conducted as described above in Examples 2 and 5. As(V) breakthrough curves for the GFO and the Zr-based media are shown in Figure 32. The Zr-based media reached the about 10 mg/L MCL at about 6,000 BV throughput, whereas the GFO had reached only about 40% of the MCL after about 16,000 BV.

[00109] While the disclosure has been described with reference to exemplary embodiments, it will be understood by those skilled in the art that various changes may be made and equivalents may be substituted for elements thereof without departing from the scope of the disclosure. In addition, many modifications may be made to adapt a particular situation or material to the teachings of the disclosure without departing from the essential scope thereof. Therefore, it is intended that the disclosure not be limited to the particular embodiment disclosed as the best mode contemplated for carrying out this disclosure, but that the disclosure will include all embodiments falling within the scope of the appended claims.

[00110] Also, as used herein, the terms "first", "second", and the like do not denote any order or importance, but rather are used to distinguish one element from another, and the terms "the", "a", and "an" do not denote a limitation of quantity, but rather denote the presence of at least one of the referenced item. Furthermore, all ranges directed to the same quantity of a given component or measurement are inclusive of the endpoints and independently combinable.

CLAIMS

1. A water treatment composition, comprising:

an oxidizing component; and

an absorbing component, wherein one or both of the oxidizing component and absorbing component comprise nanostructured materials.

2. The water treatment composition of Claim 1, wherein the one or both of the oxidizing component and absorbing component comprising the nanostructured materials are agglomerated to form particles having an average longest dimension of at least one micrometer.

3. The water treatment composition of any of the preceding Claims, wherein the oxidizing component comprises a manganese-, silver-, and/or titanium-containing composition.

4. The water treatment composition of any of the preceding Claims, wherein the oxidizing component comprises an oxide, hydroxide, or oxyhydroxide.

5. The water treatment composition of any of the preceding Claims, wherein the absorbing component comprises a titanium-, zirconium-, aluminum-, and/or iron-containing composition.

6. The water treatment composition of any of the preceding Claims, wherein the absorbing component comprises an oxide, hydroxide, or oxyhydroxide.

7. The water treatment composition of any of the preceding Claims, wherein the absorbing component is doped.

8. The water treatment composition of any of the preceding Claims, wherein the oxidizing component is doped.

9. The water treatment composition of any of the preceding Claims, wherein the oxidizing component comprises a manganese oxide, an iron-doped manganese oxide, or a combination comprising at least one of the foregoing.

10. The water treatment composition of any of the preceding Claims, wherein the absorbing component comprises an iron oxide, manganese-doped iron oxide, lanthanum-doped iron oxide, zirconium hydroxide, manganese-doped zirconium hydroxide, iron-doped zirconium hydroxide, titanium hydroxide, manganese-doped titanium hydroxide, iron-doped titanium hydroxide, or a combination comprising at least one of the foregoing.

11. The water treatment composition of any of the preceding Claims, further comprising a carrier onto which the oxidizing component and/or the absorbing component is disposed.

12. The water treatment composition of any of the preceding Claims, further comprising a filtration medium into which the oxidizing component and/or the absorbing component is embedded.

13. A water treatment composition, comprising:

a nanostructured manganese containing composition; and

a nanostructured absorbing component, wherein the nanostructure manganese-containing composition and the nanostructured absorbing component are agglomerated to form a particle having an average longest dimension of at least one micrometer.

14. The water treatment composition of Claim 13, wherein the nanostructured manganese containing composition is a manganese oxide, an iron-doped manganese oxide, or a combination comprising at least one of the foregoing.

15. The water treatment composition of any of the preceding Claims, wherein the nanostructured absorbing component comprises a titanium-, zirconium-, aluminum-, and/or iron-containing composition.

16. The water treatment composition of any of the preceding Claims, wherein the nanostructured absorbing component comprises an iron oxide, manganese-doped iron oxide, lanthanum-doped iron oxide, zirconium hydroxide, manganese-doped zirconium hydroxide, iron-doped zirconium hydroxide, titanium hydroxide, manganese-doped titanium hydroxide, iron-doped titanium hydroxide, or a combination comprising at least one of the foregoing.

17. The water treatment composition of any of the preceding Claims, further comprising a carrier onto which the oxidizing component and/or the absorbing component is disposed.

18. The water treatment composition of any of the preceding Claims, further comprising a filtration medium into which the oxidizing component and/or the absorbing component is embedded.

19. A method for treating water, comprising

contacting water with a water treatment composition of any of Claims 1 through 12; and

at least partially removing a contaminant from the water.

20. The method of Claim 19, wherein the at least partially removing a contaminant comprises:

oxidizing the contaminant; and

absorbing the oxidized contaminant.

21. The method of any of the preceding Claims, wherein the contaminant comprises metallic or cationic arsenic, lead, mercury, chromium, or a combination comprising at least one of the foregoing.

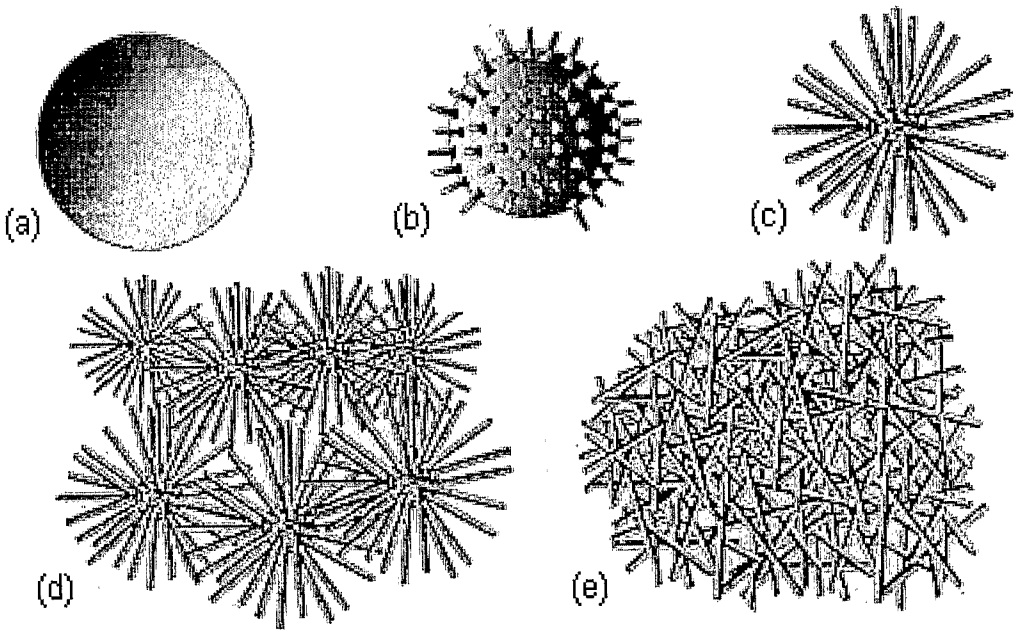

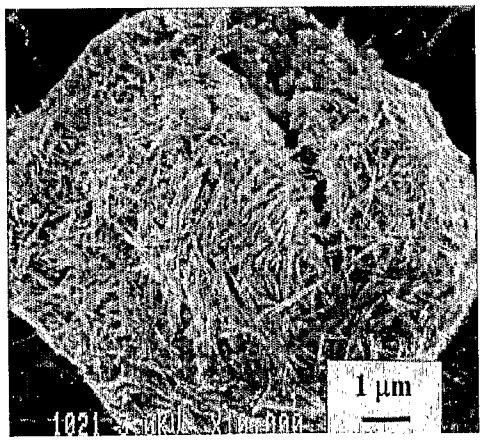

(f)

FIGURE 1

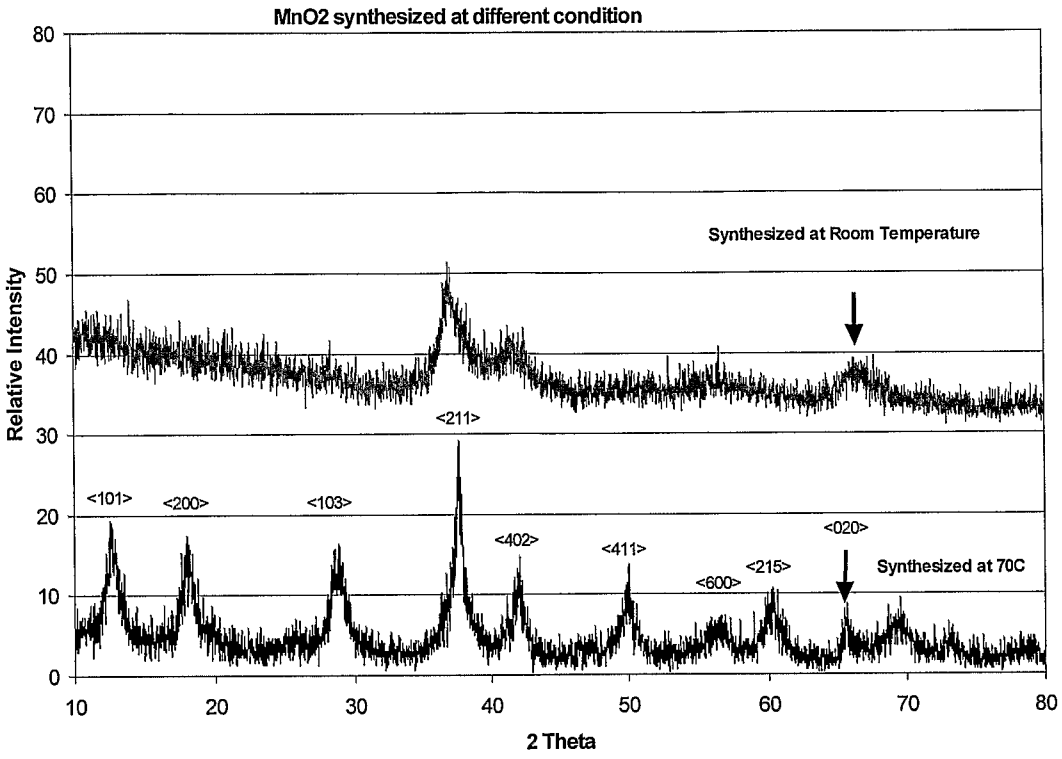
MnO2 synthesized at different condition
Relative Intensity
2 Theta
Synthesized at Room Temperature
Synthesized at 70C
<101>
<200>
<103>
<211>
<402>
<411>
<600>
<215>
<020>
0
10
20
30
40
50
60
70
80

FIGURE 2

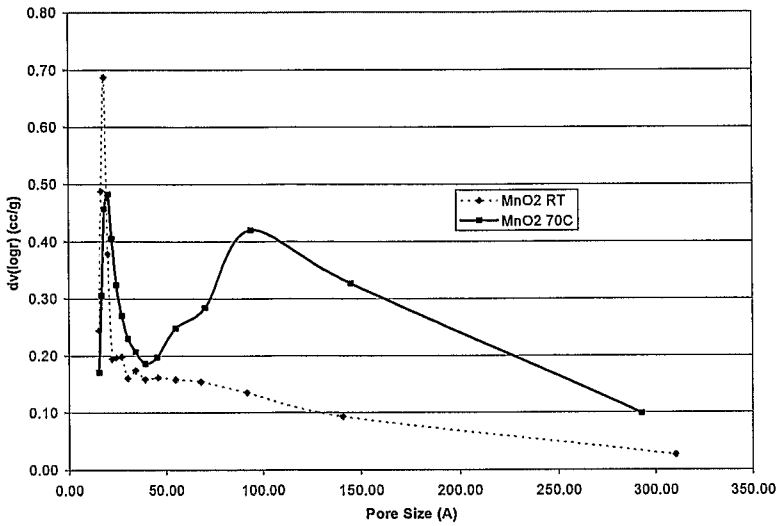

FIGURE 3

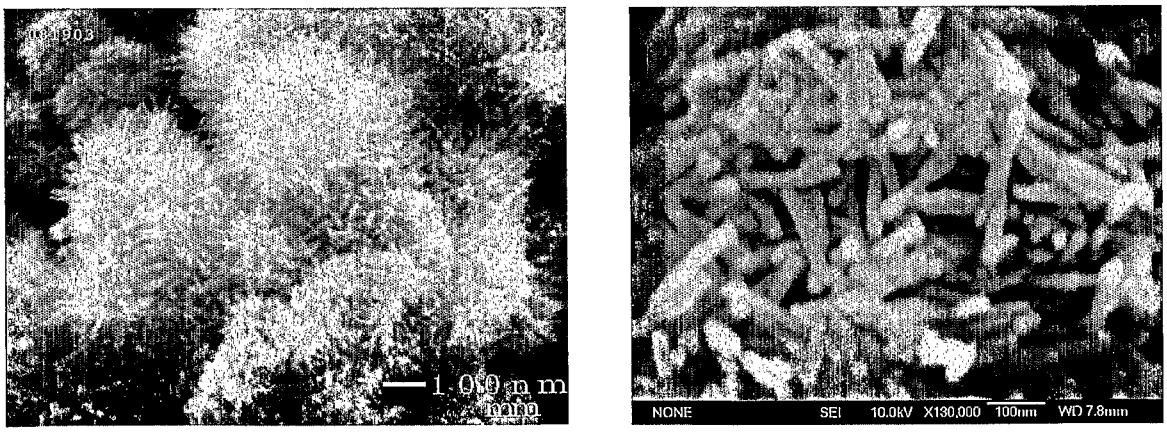

(a) (b)

FIGURE 4

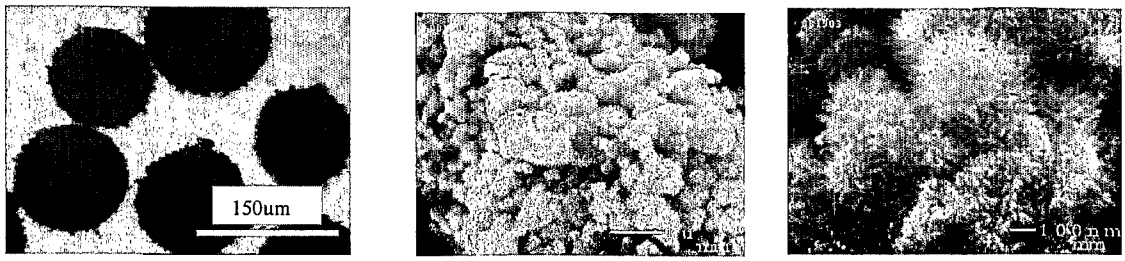

(a) (b) (c)

FIGURE 5

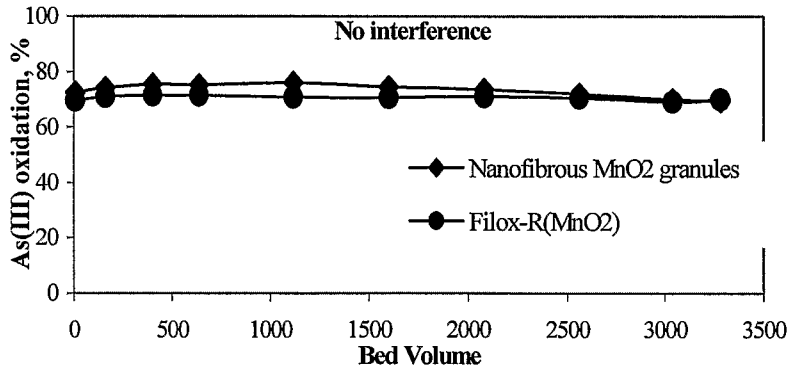

FIGURE 6

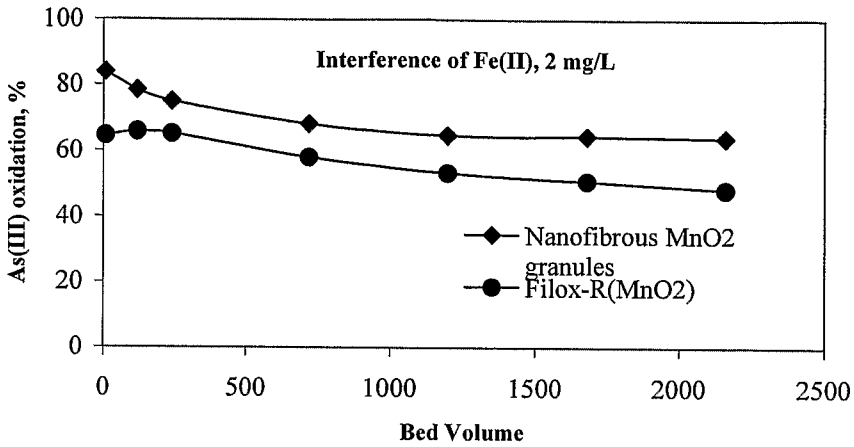

FIGURE 7

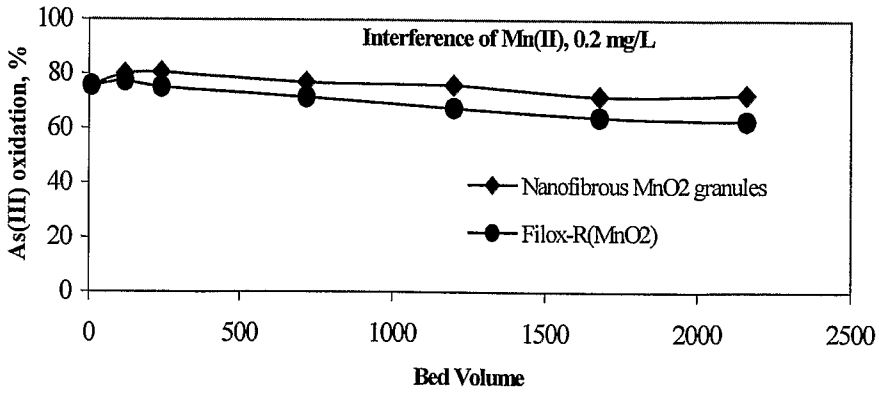

FIGURE 8

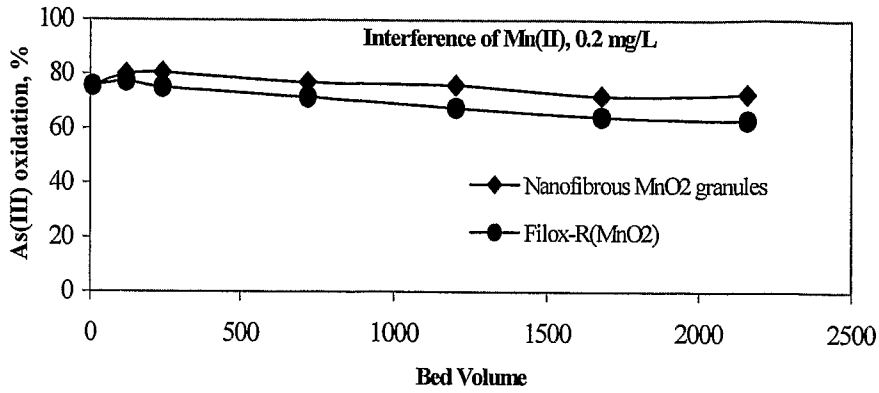

FIGURE 9

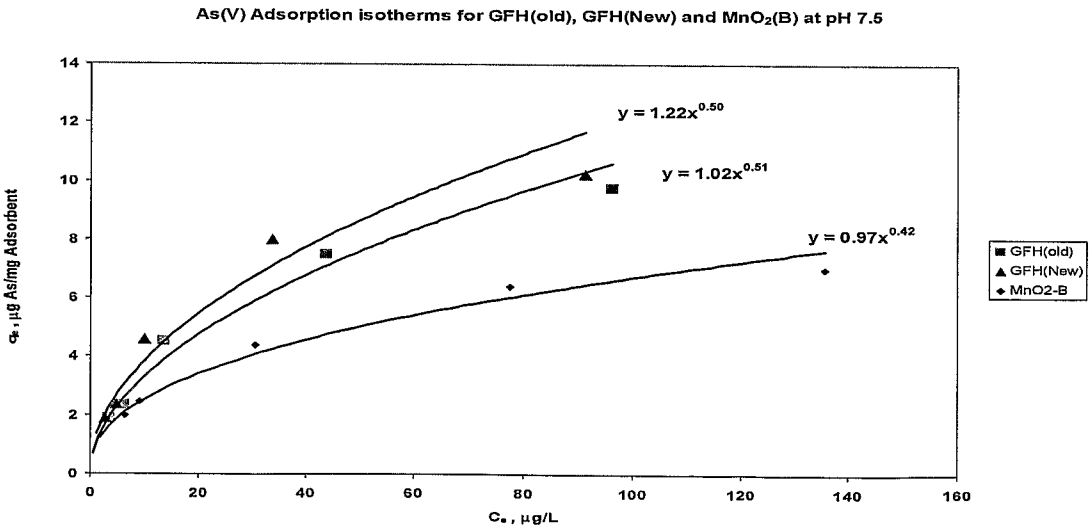

FIGURE 10

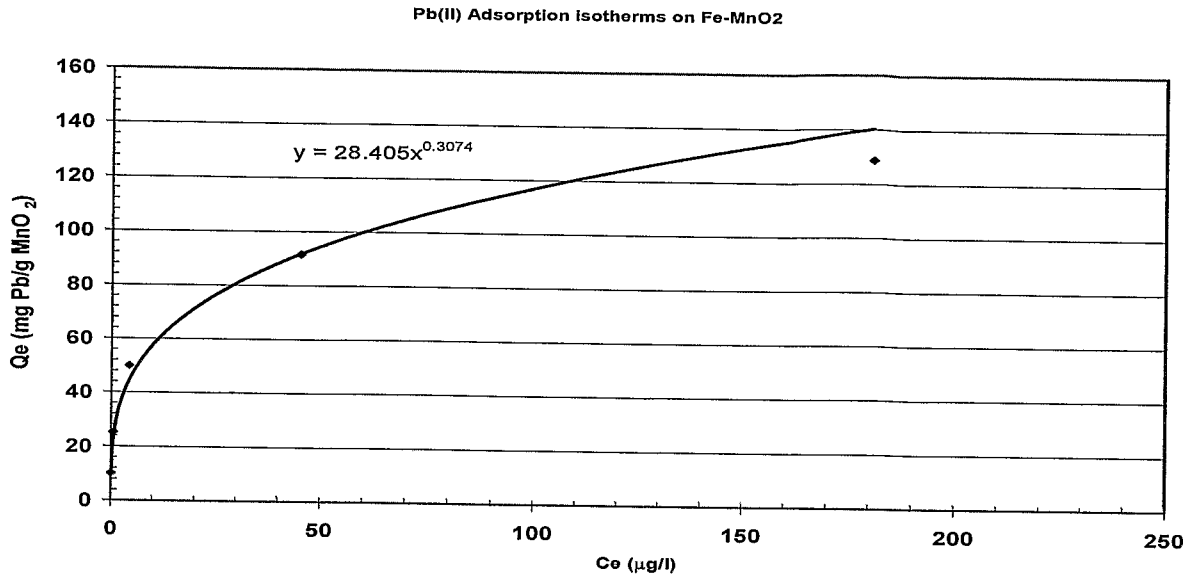
Pb(II) Adsorption Isotherms on Fe-MnO2
y = 28.405x^0.3074
Qe (mg Pb/g MnO 2)
Ce (µg/l)
0
20
40
60
80
100
120
140
160
0
50
100
150
200
250

FIGURE 11

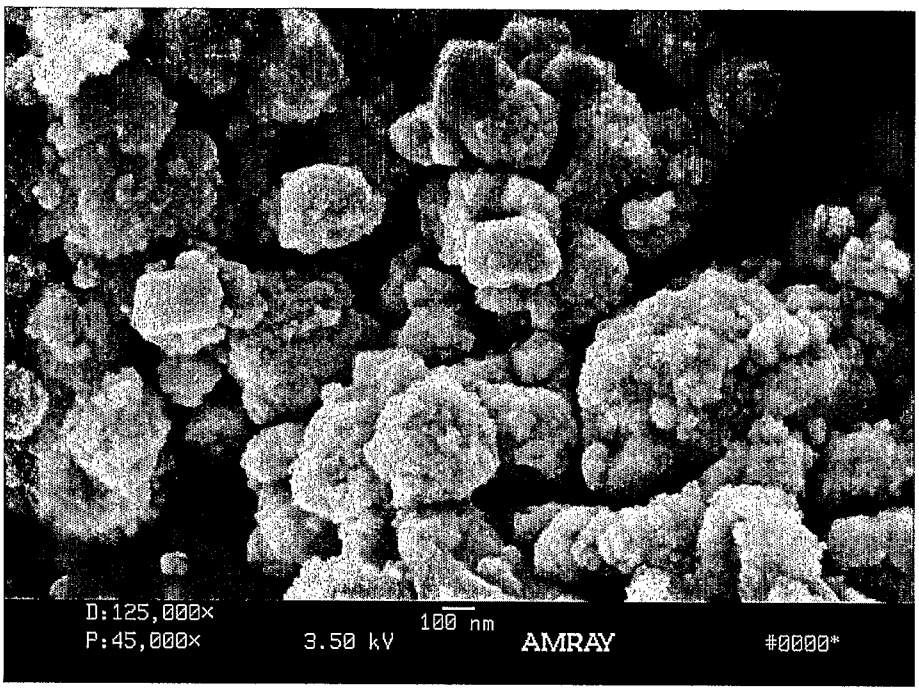

FIGURE 12

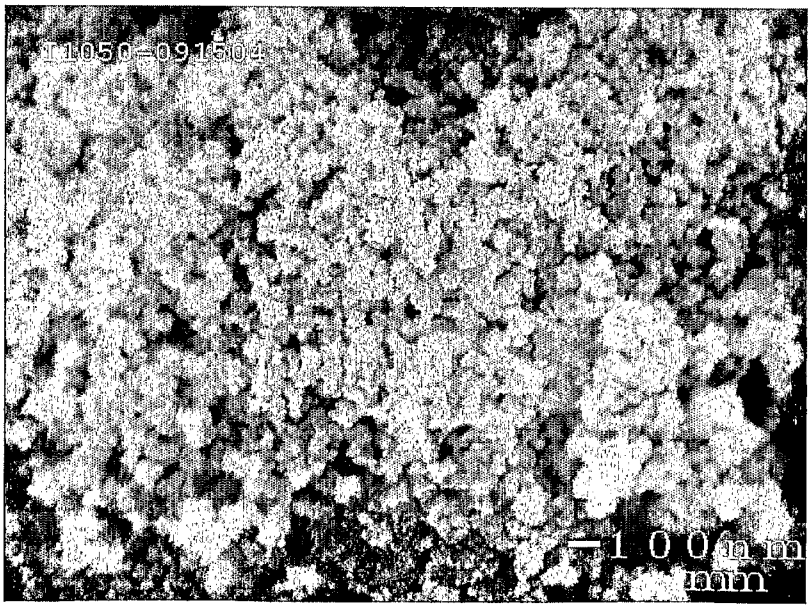

FIGURE 13

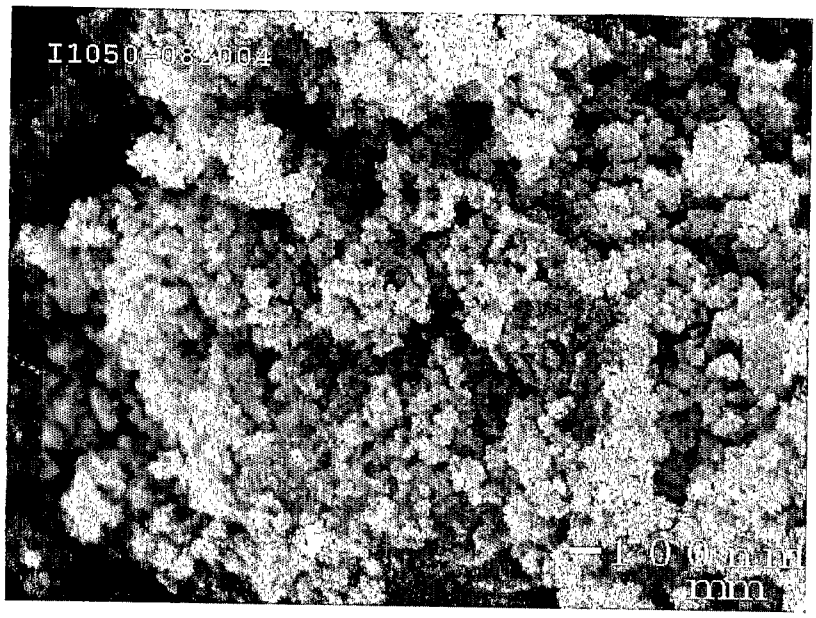

FIGURE 14

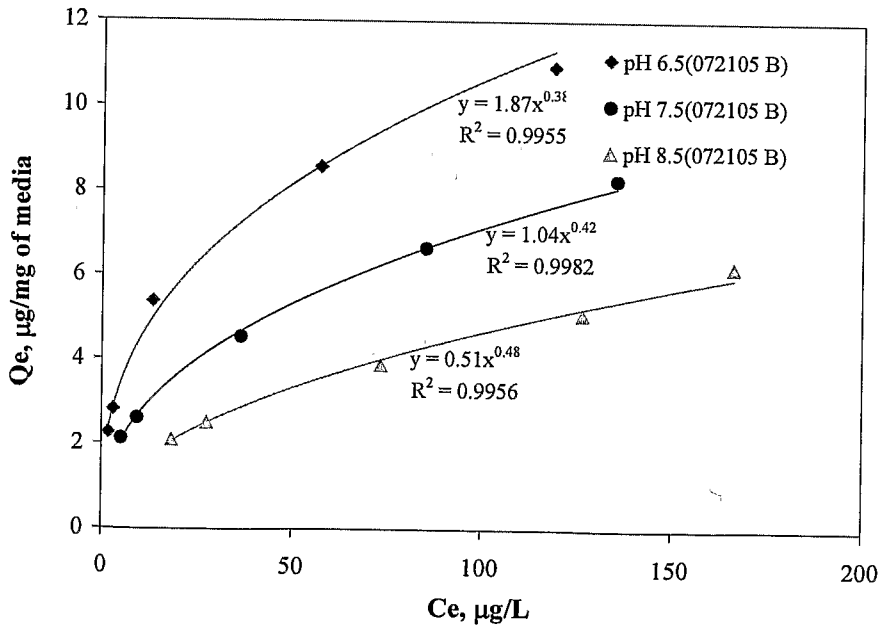

FIGURE 15

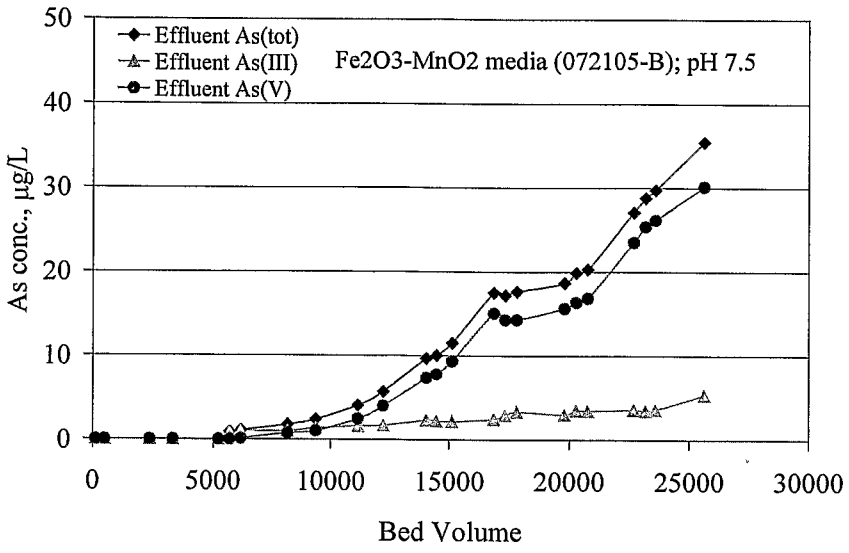

FIGURE 16

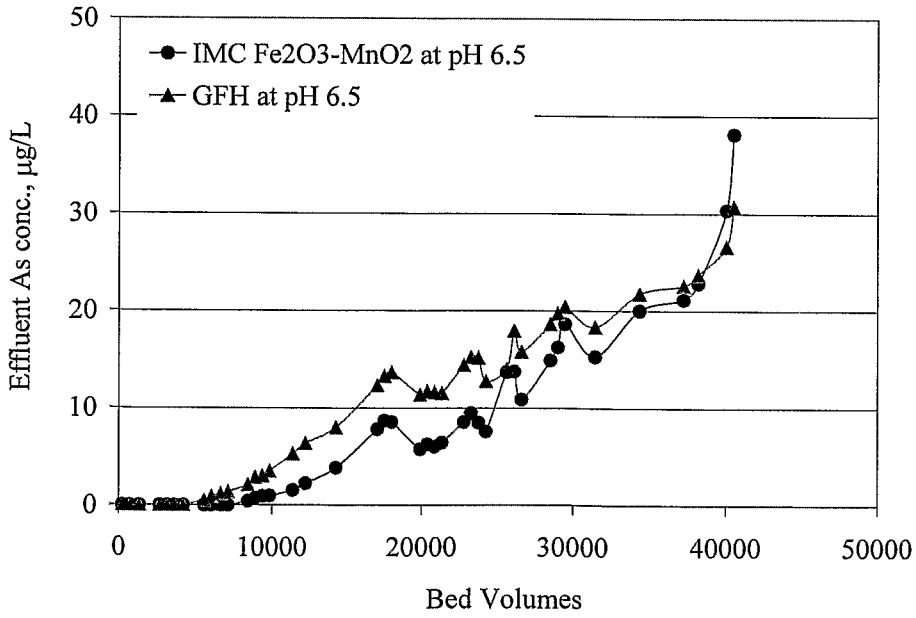

FIGURE 17

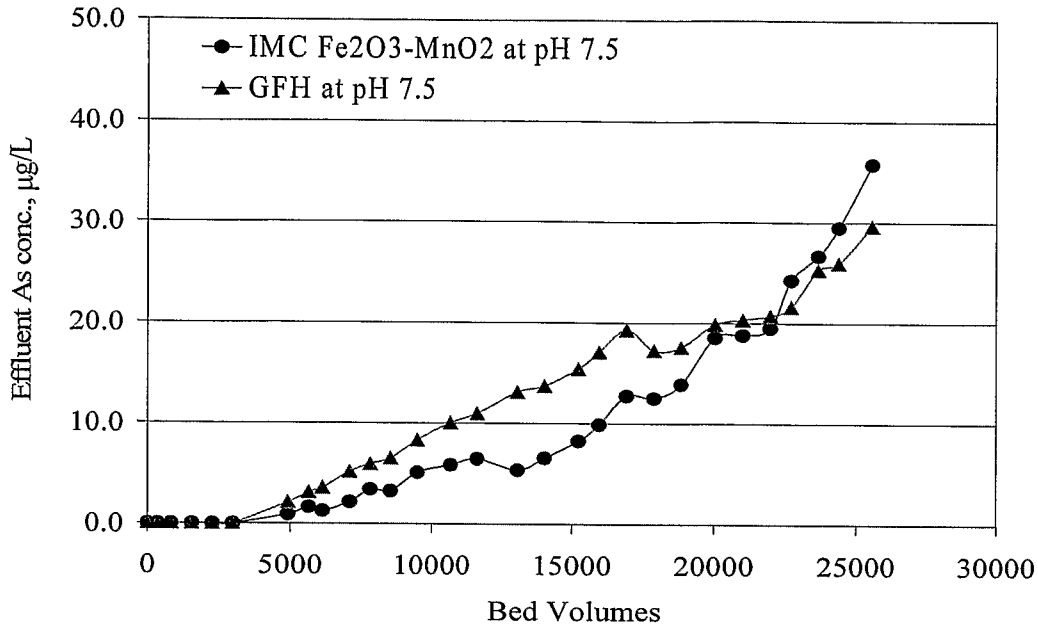

FIGURE 18

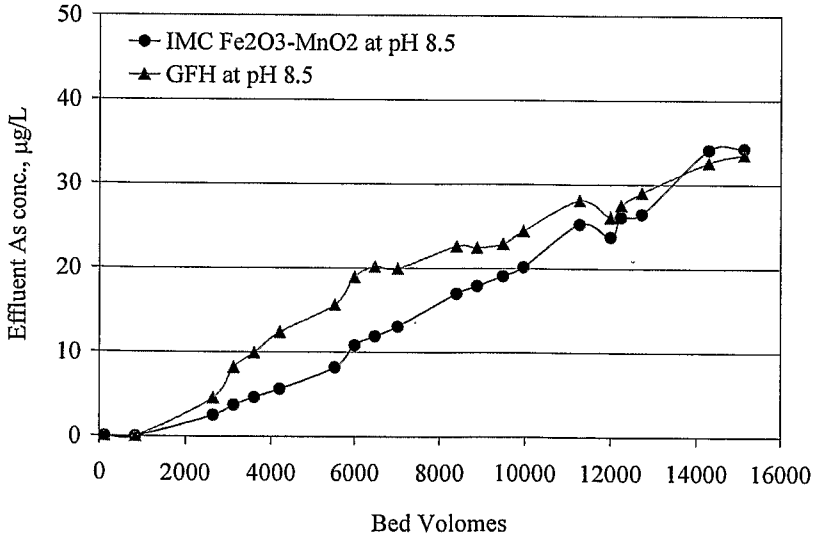

FIGURE 19

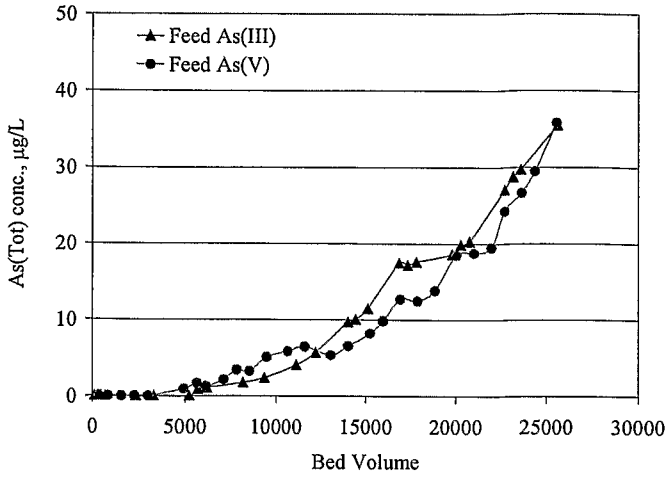

FIGURE 20

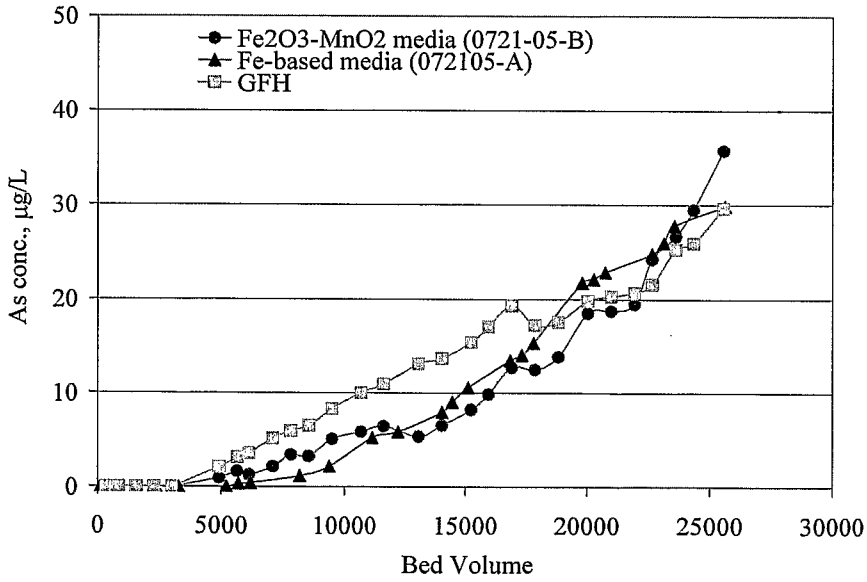

FIGURE 21

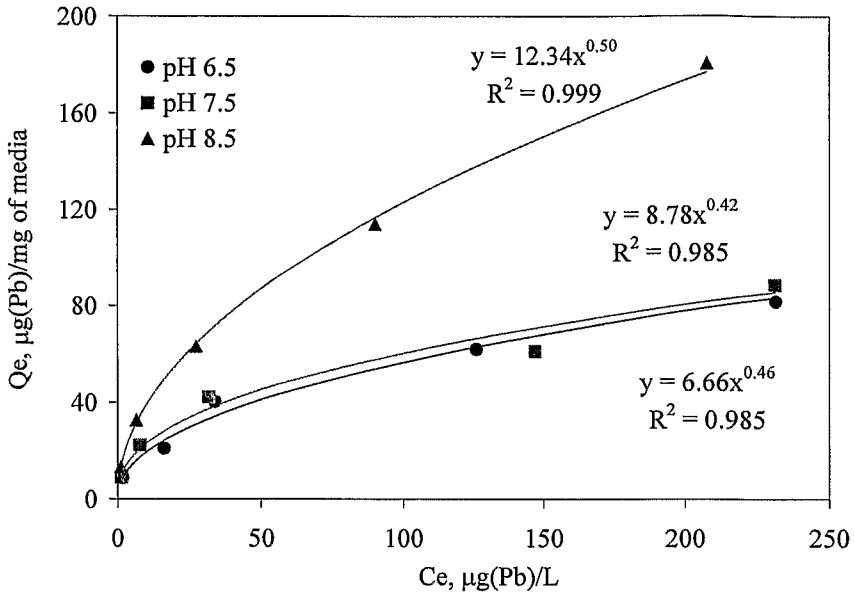

FIGURE 22

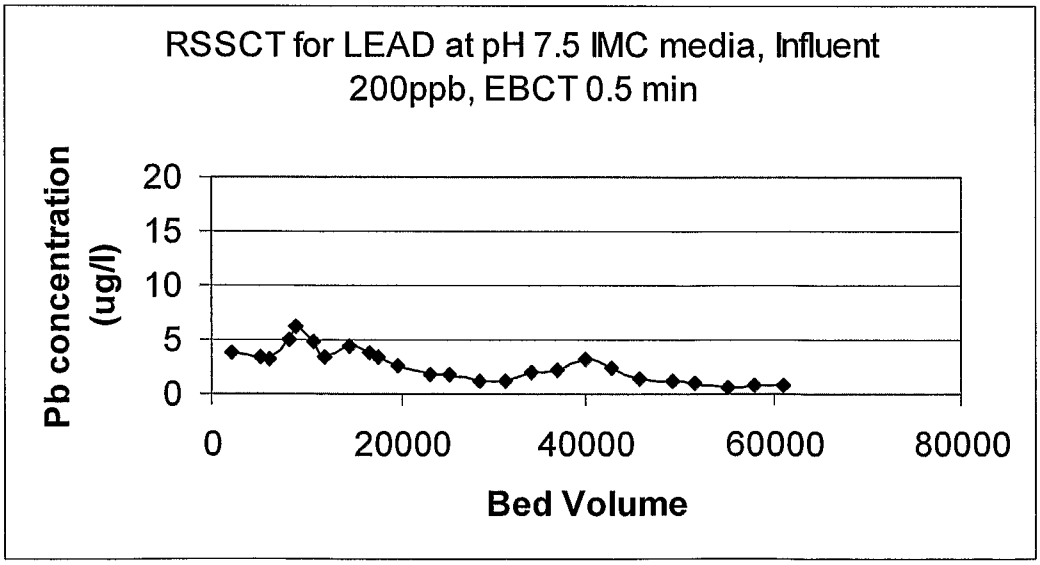

FIGURE 23

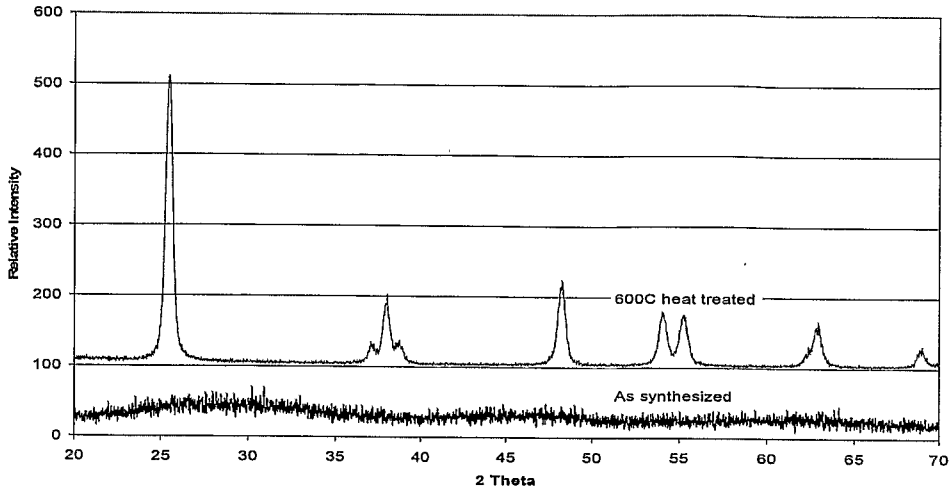

FIGURE 24

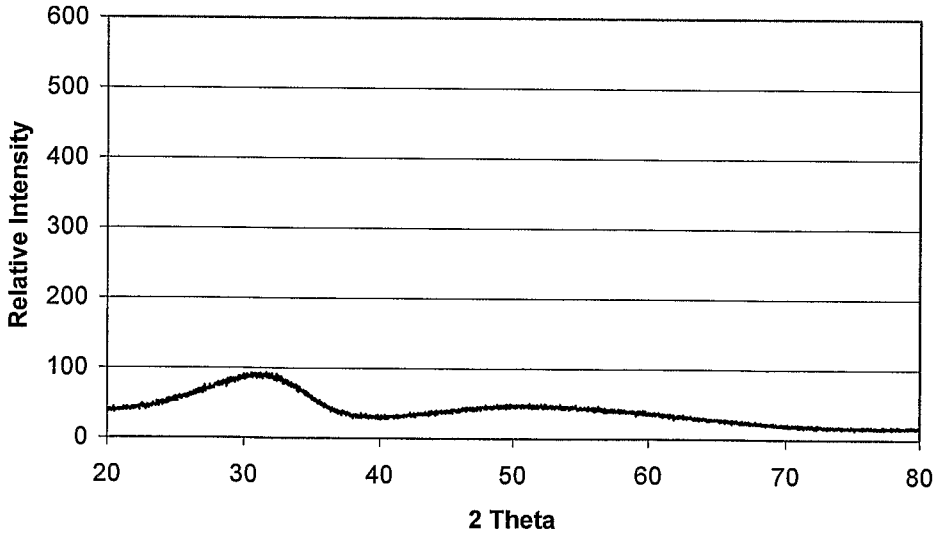

FIGURE 25

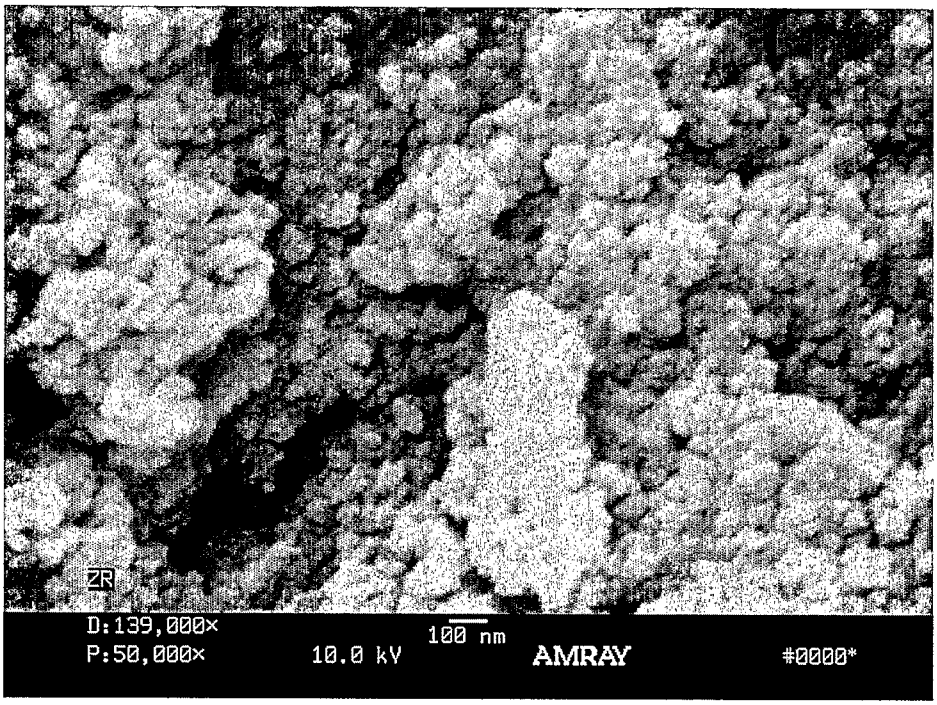

FIGURE 26

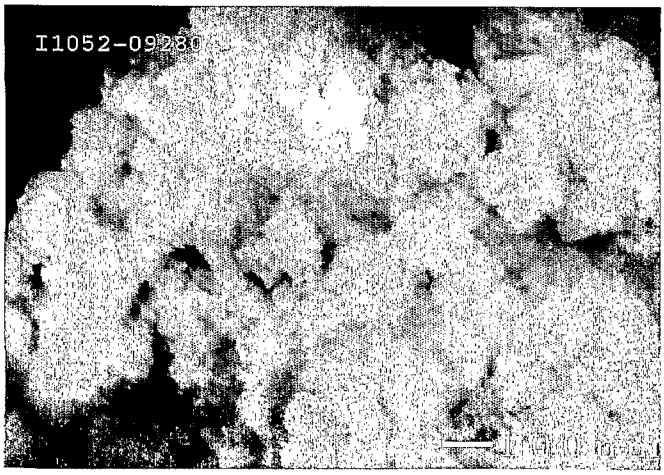

FIGURE 27

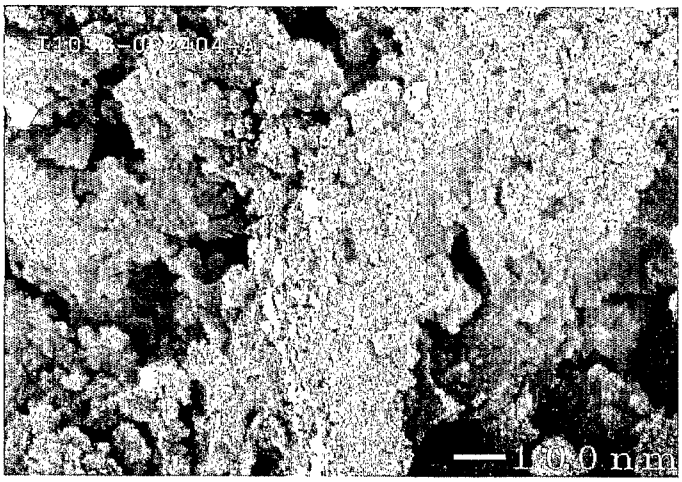

FIGURE 28

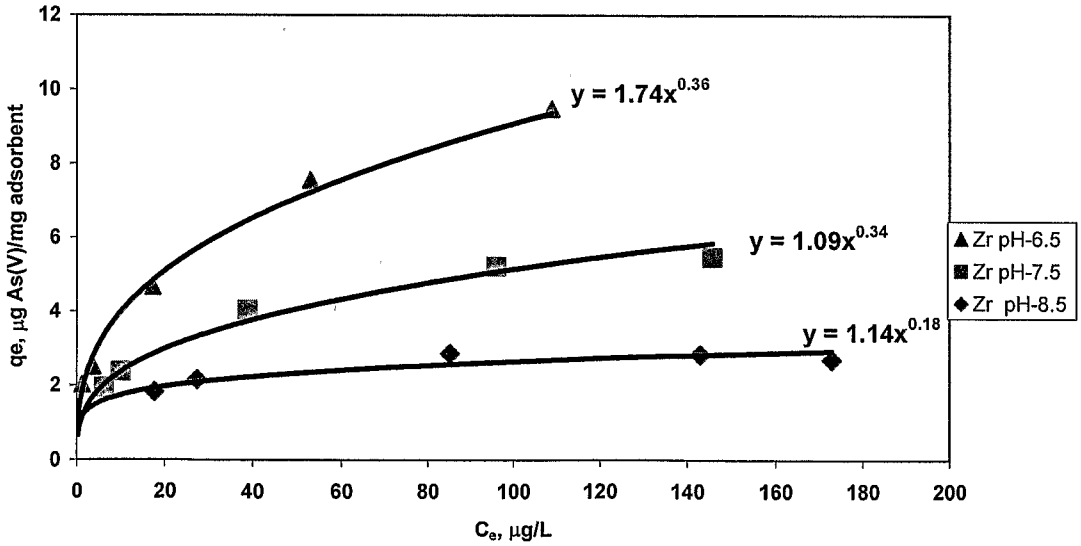

FIGURE 29

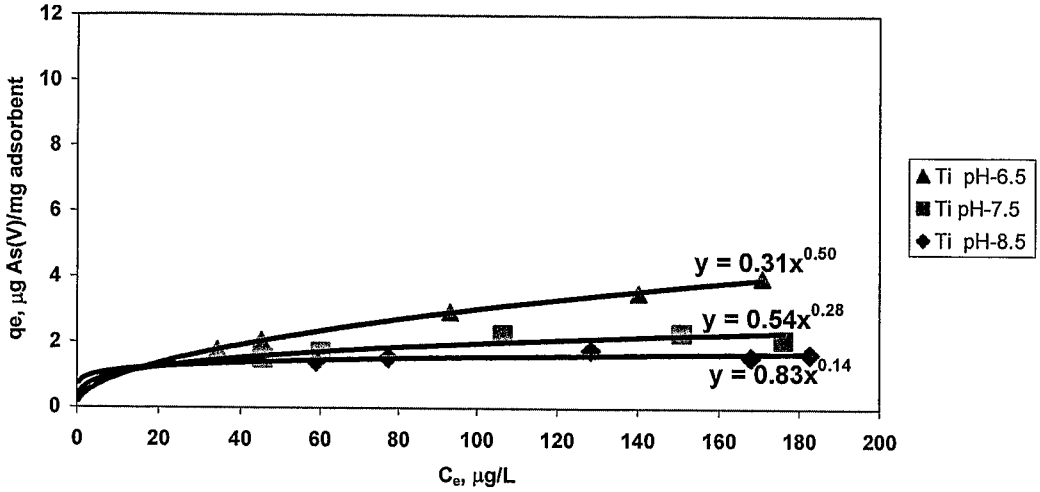

FIGURE 30

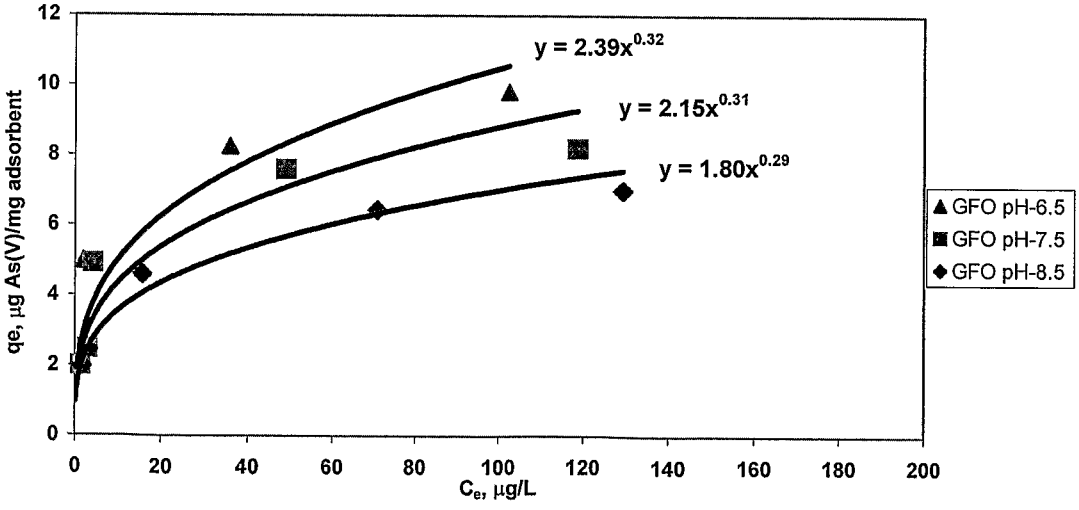

FIGURE 31

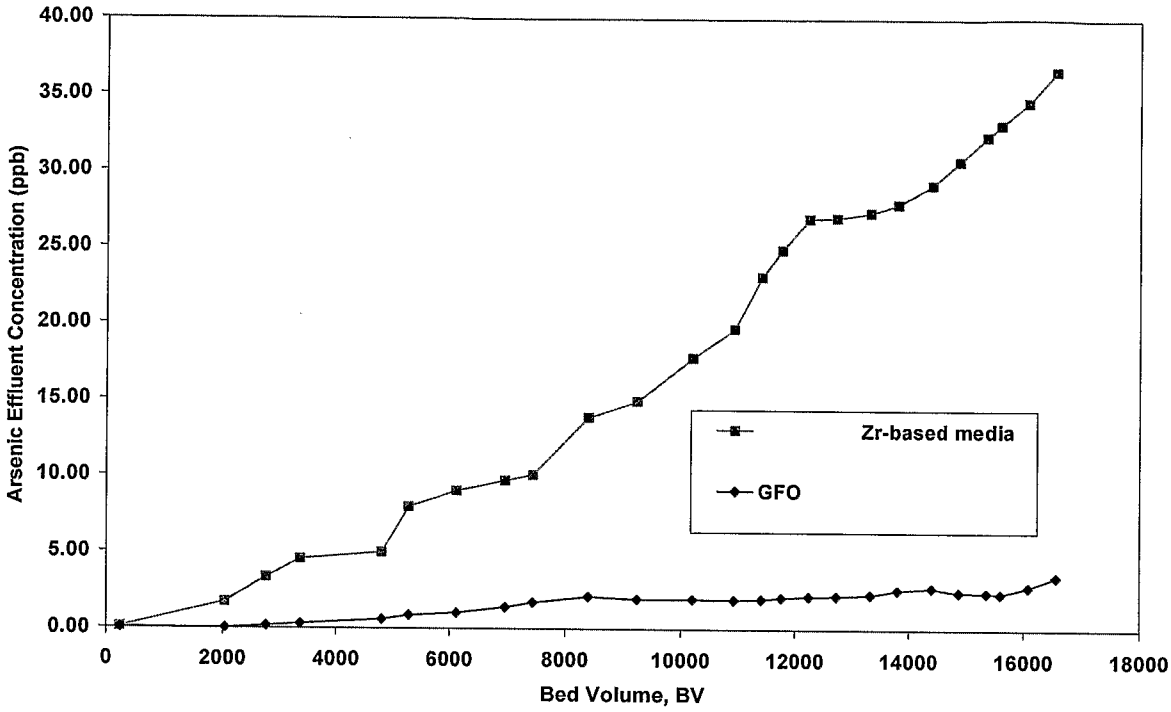
40.00
35.00
30.00
25.00
20.00
15.00
10.00
5.00
0.00
Arsenic Effluent Concentration (ppb)
0
2000
4000
6000
8000
10000
12000
14000
16000
18000
Bed Volume, BV
Zr-based media
GFO

FIGURE 32

INTERNATIONAL SEARCH REPORT

International application No
PCT/US2006/040458

A. CLASSIFICATION OF SUBJECT MATTER
INV. C02F1/72 C02F1/28 C02F1/62

According to International Patent Classification (IPC) or to both national classification and IPC

B. FIELDS SEARCHED

Minimum documentation searched (classification system followed by classification symbols)
C02F

Documentation searched other than minimum documentation to the extent that such documents are included in the fields searched

Electronic data base consulted during the international search (name of data base and, where practical, search terms used)
EPO-Internal, WPI Data

C. DOCUMENTS CONSIDERED TO BE RELEVANT

Category*	Citation of document, with indication, where appropriate, of the relevant passages	Relevant to claim No.
X	WO 2004/032624 A (NANOSCALE MATERIALS INC) 22 April 2004 (2004-04-22) page 1, line 6 - line 16; claims 1-26 page 2, line 28 - page 4, line 27	1-12, 19-21
X	WO 2004/076364 A (THE PUR WATER PURIFICATION PRODCUS INC) 10 September 2004 (2004-09-10) page 1, paragraph 1; claims 1-36 page 7, paragraph 2 - page 8, paragraph 3 page 27, paragraph 3	1-12, 19-21
Y	US 2004/065619 A1 (KLABUNDE KENNETH J [US] ET AL) 8 April 2004 (2004-04-08) page 1, paragraph 1 - paragraph 5; claims 1-49 page 1, paragraph 8	1-12, 19-21

-/--

[X] Further documents are listed in the continuation of Box C.

[X] See patent family annex.

* Special categories of cited documents :

"A" document defining the general state of the art which is not considered to be of particular relevance

"E" earlier document but published on or after the international filing date

"L" document which may throw doubts on priority claim(s) or which is cited to establish the publication date of another citation or other special reason (as specified)

"O" document referring to an oral disclosure, use, exhibition or other means

"P" document published prior to the international filing date but later than the priority date claimed

"T" later document published after the international filing date or priority date and not in conflict with the application but cited to understand the principle or theory underlying the invention

"X" document of particular relevance; the claimed invention cannot be considered novel or cannot be considered to involve an inventive step when the document is taken alone

"Y" document of particular relevance; the claimed invention cannot be considered to involve an inventive step when the document is combined with one or more other such documents, such combination being obvious to a person skilled in the art.

"&" document member of the same patent family

Date of the actual completion of the international search	Date of mailing of the international search report
9 March 2007	28/03/2007

Name and mailing address of the ISA/	Authorized officer
European Patent Office, P.B. 5818 Patentlaan 2 NL - 2280 HV Rijswijk Tel. (+31-70) 340-2040, Tx. 31 651 epo nl, Fax: (+31-70) 340-3016	Oenhausen, Claudia

Form PCT/ISA/210 (second sheet) (April 2005)

INTERNATIONAL SEARCH REPORT

International application No
PCT/US2006/040458

C(Continuation). DOCUMENTS CONSIDERED TO BE RELEVANT

Category*	Citation of document, with indication, where appropriate, of the relevant passages	Relevant to claim No.
Y	US 6 764 601 B1 (LEVY EHUD [US] ET AL) 20 July 2004 (2004-07-20) column 1, line 5 - line 27; claims 1-15 column 4, line 31 - line 57 column 8, line 50 - column 9, line 4	1-12, 19-21
Y	WO 03/068683 A (TRUSTEES OF STEVENS INST OF TE [US]; MENG XIAOGUANG [US]; DADACHOV MAZ) 21 August 2003 (2003-08-21) page 1, paragraph 1; claims 1-49 page 4, paragraph 3 - page 6, paragraph 2 page 10, paragraph 2	1-12, 19-21
P,A	WO 2006/065825 A2 (UNIV HAWAII [US]; RIMA JAMIL [LB]; LI QING X [US]; AOUEZOVA LIZETTE [L) 22 June 2006 (2006-06-22) page 35, paragraph 147 - page 36, paragraph 148; claims 1-24	1-21
A	SCHMIDT, K- ET AL.: "Nanotechnology in the environment industry: opportunities and trends" FINAL REPORT AND BIBLIOGRAPHY FOR THE NANO-ENVIRONMENTAL CROSS-SECTOR INITIATIVE, 4 March 2005 (2005-03-04), XP002423932 Alberta, USA the whole document	1-21

3

INTERNATIONAL SEARCH REPORT

Information on patent family members

International application No
PCT/US2006/040458

Patent document cited in search report	Publication date	Patent family member(s)	Publication date
WO 2004032624 A	22-04-2004	AU 2003291633 A1	04-05-2004
		CA 2501804 A1	22-04-2004
		EP 1560486 A2	10-08-2005
		JP 2006501962 T	19-01-2006
		US 2004067159 A1	08-04-2004
WO 2004076364 A	10-09-2004	AU 2004215404 A1	10-09-2004
		BR PI0407450 A	24-01-2006
		CA 2516582 A1	10-09-2004
		CN 1750997 A	22-03-2006
		EP 1601618 A1	07-12-2005
		JP 2006518339 T	10-08-2006
		KR 20050107759 A	15-11-2005
		MA 27659 A1	01-12-2005
		MX PA05008863 A	17-02-2006
		US 2004164029 A1	26-08-2004
US 2004065619 A1	08-04-2004	NONE	
US 6764601 B1	20-07-2004	NONE	
WO 03068683 A	21-08-2003	AU 2003211074 A1	04-09-2003
		DE 10392330 T5	24-02-2005
		GB 2400843 A	27-10-2004
		GB 2424221 A	20-09-2006
		JP 2005517521 T	16-06-2005
		MX PA04007805 A	20-06-2005
		US 2006091078 A1	04-05-2006
		US 2006091079 A1	04-05-2006
		US 2003155302 A1	21-08-2003
WO 2006065825 A2	22-06-2006	NONE	